

**NASA TECHNICAL  
MEMORANDUM**



**NASA TM X-3329**

**NASA TM X-3329**

**AMES COLLABORATIVE STUDY  
OF COSMIC RAY NEUTRONS**

*J. E. Hewitt, L. Hughes, J. B. McCaslin,  
L. D. Stephens, A. Rindi, A. R. Smith,  
R. H. Thomas, R. V. Griffith, C. G. Welles,  
J. W. Baum, and A. V. Kuebner*

*Ames Research Center  
Moffett Field, Calif. 94035*



**NATIONAL AERONAUTICS AND SPACE ADMINISTRATION • WASHINGTON, D. C. • JANUARY 1976**

1. Report No. NASA TM X-3329		2. Government Accession No.		3. Recipient's Catalog No.	
4. Title and Subtitle AMES COLLABORATIVE STUDY OF COSMIC RAY NEUTRONS				5. Report Date January 1976	
				6. Performing Organization Code	
7. Author(s) J. E. Hewitt,* L. Hughes,* J. B. McCaslin,† L. D. Stephens,† A. Rindi,† A. R. Smith,† R. H. Thomas,† R. V. Griffith,‡ C. G. Welles,§ J. W. Baum,¶ and A. V. Kuehner¶				8. Performing Organization Report No. A-6139	
				10. Work Unit No. 970-21-63	
9. Performing Organization Name and Address *Ames Research Center, Moffett Field, Calif. 94035 †Lawrence Berkeley Laboratory, University of California, Berkeley, Calif. 94720 ‡Lawrence Livermore Laboratory, University of California, Livermore, Calif. 94550 §San Jose State University, San Jose, Calif. 95192 ¶Brookhaven National Laboratory, Long Island, N. Y.				11. Contract or Grant No.	
				13. Type of Report and Period Covered Technical Memorandum	
				14. Sponsoring Agency Code	
12. Sponsoring Agency Name and Address National Aeronautics and Space Administration Washington, D. C. 20546					
15. Supplementary Notes					
16. Abstract <p>Hess and his co-workers made one of the first measurements of the cosmic-ray neutron differential energy spectrum. They determined the spectrum between 0.01 eV and 10 GeV at several aircraft altitudes. More recent data cast doubt on both the reported flux intensities and the spectral shape. In particular, the existence of a broad evaporation peak near 1 MeV is questioned and it is suggested that a larger fraction of the flux (and hence the contribution to the dose) consists of neutrons with energies greater than 10 MeV.</p> <p>This report describes the results of a collaborative study to define both the flux and the spectrum more precisely and to develop a dosimetry package that can be flown quickly to altitude for solar flare events. Instrumentation and analysis techniques are used which were developed to measure accelerator-produced radiation. The instruments are flown in the Ames Research Center high-altitude aircraft. Neutron instrumentation consists of Bonner spheres with both active and passive detector elements, threshold detectors of both prompt-counter and activation-element types, a liquid scintillation spectrometer (developed by New York University) based on pulse-shape discrimination, and a moderated BF<sub>3</sub> counter neutron monitor. In addition, charged particles are measured with a Reuter-Stokes ionization chamber system and dose equivalent with an instrument on loan from Brookhaven National Laboratory. Preliminary results from the first series of flights at 12.5 km (41,000 ft) are presented, including estimates of total neutron flux intensity and spectral shape and of the variation of intensity with altitude and geomagnetic latitude.</p>					
17. Key Words (Suggested by Author(s)) Space radiation Radiation at aircraft altitudes Atmospheric neutron spectrum				18. Distribution Statement Unlimited  STAR Category - 93	
19. Security Classif. (of this report) Unclassified		20. Security Classif. (of this page) Unclassified		21. No. of Pages 39	22. Price* \$3.75

## AMES COLLABORATIVE STUDY OF COSMIC RAY NEUTRONS

J. E. Hewitt,\* L. Hughes,\* J. B. McCaslin,† L. D. Stephens,†  
A. Rindi,† A. R. Smith,† R. H. Thomas,† R. V. Griffith,‡  
C. G. Welles,§ J. W. Baum,¶ and A. V. Kuehner¶

### SUMMARY

Hess and his co-workers made one of the first measurements of the cosmic-ray neutron differential energy spectrum. They determined the spectrum between 0.01 eV and 10 GeV at several aircraft altitudes. More recent data cast doubt on both the reported flux intensities and the spectral shape. In particular, the existence of a broad evaporation peak near 1 MeV is questioned and it is suggested that a larger fraction of the flux (and hence the contribution to the dose) consists of neutrons with energies greater than 10 MeV.

This report describes the results of a collaborative study to define both the flux and the spectrum more precisely and to develop a dosimetry package that can be flown quickly to altitude for solar flare events. Instrumentation and analysis techniques are used which were developed to measure accelerator-produced radiation. The instruments are flown in the Ames Research Center high-altitude aircraft. Neutron instrumentation consists of Bonner spheres with both active and passive detector elements, threshold detectors of both prompt-counter and activation-element types, a liquid scintillation spectrometer (developed by New York University) based on pulse-shape discrimination, and a moderated BF<sub>3</sub> counter neutron monitor. In addition, charged particles are measured with a Reuter-Stokes ionization chamber system and dose equivalent with an instrument on loan from Brookhaven National Laboratory. Preliminary results from the first series of flights at 12.5 km (41,000 ft) are presented, including estimates of total neutron flux intensity and spectral shape and of the variation of intensity with altitude and geomagnetic latitude.

### INTRODUCTION

At sea level, neutrons contribute about 10 percent of the total radiation exposure to man from cosmic rays (ref. 1). Neutrons reaching the Earth's surface are principally created in the Earth's atmosphere by the interaction of the primary cosmic rays with oxygen and nitrogen nuclei at high altitudes and in the subsequent development of a hadronic cascade down through the atmosphere. (Relatively few neutrons are present in the primary galactic cosmic radiation or solar radiation reaching the Earth because their radioactive half-life is approximately 12 min.) Two nuclear reactions are important in the production of cosmic-ray neutrons: direct inelastic reactions producing "knock-on" neutrons, with energies from about 1 MeV to well in excess of 1 GeV, and evaporation

---

\* Ames Research Center, Moffett Field, Calif. 94035.

† Health Physics Dept., Lawrence Berkeley Laboratory, University of California, Berkeley, Calif. 94720.

‡ Hazards Control Section, Lawrence Livermore Laboratory, University of California, Livermore, Calif. 94550.

§ Physics Dept., San Jose State University, San Jose, Calif. 95192.

¶ Brookhaven National Laboratory, Long Island, N. Y.

processes in which neutrons peaked around 1 MeV are emitted in the de-excitation of nuclei following inelastic processes (ref. 2).

The atmospheric neutron intensity depends on the intensity of charged particles reaching the atmosphere, which in turn depends on the strength of the Earth's magnetic field. Consequently, the neutron flux density increases with geomagnetic latitude because charged particles of lower momentum may enter the atmosphere. In periods of high solar activity, the Earth's magnetic field is modified by the Sun and the atmospheric neutron flux density is generally decreased (ref. 3). However, during a solar flare, protons emitted by the Sun reach the Earth and can increase the neutron flux density dramatically over a period of several hours or even days.

The study of these cosmic-ray neutrons is of both practical and fundamental interest. Interactions of the primary cosmic rays with the atmosphere and the subsequent generation of hadronic and electromagnetic cascades have been studied both experimentally and theoretically for many years.

In 1959, Hess et al. (ref. 4) reported one of the first measurements of the energy spectrum of cosmic-ray neutrons in the energy region between 0.01 eV and 10 GeV at several altitudes. One significant feature of their spectrum is a peak at a few MeV, attributed by the authors to nuclear evaporation processes. Only a few measurements of neutron spectra have been reported since then and the most recent do not extend over as wide an energy range as that of Hess et al. Thus Preszler et al. (ref. 5) reported a measurement using scintillators in the energy range between 10 and 100 MeV at an altitude of 40 km (130,000 ft). Kanbach et al. (ref. 6) reported a measurement using a spark chamber spectrometer that determined the spectrum between 70 and 250 MeV at an atmosphere depth of  $5 \text{ g cm}^{-2}$ . Jenkins et al. (ref. 7) used a  $^3\text{He}$  proportional counter to determine the neutron spectrum in the range 10 keV to 10 MeV aboard a satellite. The most recent measurement comparable with that of Hess et al. was done by Hajnal et al. (ref. 8) using Bonner spheres. These measurements shown general agreement with the spectrum derived by Hess et al., but there are considerable differences in the literature as to the absolute neutron intensity.

At sea level, the neutron flux density is small and difficult to measure since it is easily perturbed by local terrain. Table 1 summarizes some of the more recent data. Table 1 shows differences of nearly a factor of 3. Estimates of the sea-level intensity from measurements at higher altitudes assuming an exponential variation with pressure altitude are extremely sensitive to the value of attenuation length assumed. If such extrapolated estimates are not considered, the recent measurements by Kent (ref. 13), Boella et al. (ref. 10), Yamashita et al. (ref. 14), and Hajnal et al. (ref. 8) agree to within about 30 percent for the range  $6.5 \times 10^{-3}$  to  $8.4 \times 10^{-3} \text{ n-cm}^{-2} \text{ sec}^{-1}$ . However, even this variation seems too large to be accounted for by a variation in solar activity, which has been estimated to be less than 5 percent at middle latitudes (refs. 15 and 16). Lowder et al. (ref. 17) have drawn attention to comparable discrepancies in published values of the absolute cosmic ray free air ionization. It is apparent that improvement is required even in our knowledge of absolute neutron intensity and its variation with altitude.

Increasing interest in the exposure of large populations to small levels of radiations due to man's activities has stimulated studies of the population exposure resulting from commercial aviation (ref. 3) (Wallace, private communication, 1975). Estimates of population exposures resulting from both subsonic and supersonic flights depend not only on knowledge of radiation intensity but

TABLE 1.— SUMMARY OF SEA-LEVEL COSMIC-RAY NEUTRON DATA (ref. 8)

Reference	Latitude, deg	Neutron flux density, n-cm <sup>-2</sup> sec <sup>-1</sup>
9	41	0.01
10	46	.0065
11	46	.0180 <sup>a</sup>
12	55	.0180 <sup>b</sup>
13	46	.0084
14	44	.0074
8	41	.0082

<sup>a</sup>Obtained by Watt et al. (ref. 12) extrapolating higher altitude data to sea level using 145 g/cm<sup>2</sup> relaxation length.

<sup>b</sup>Average value from the results of several investigators as extrapolated.

also on its energy spectrum. Patterson et al. (ref. 18) used the neutron spectrum measured by Hess et al. to derive the distribution of dose equivalent as a function of neutron energy. They calculated that 80 percent of the neutron dose equivalent was produced by neutrons having energies between 0.1 and 10 MeV.

Over the past several years, theoretical studies have developed techniques for calculating nuclear cascade processes, facilitating the calculation of the production and transport through the atmosphere of the electromagnetic and hadronic cascades initiated by the primary cosmic radiation. O'Brien reviewed some of the analytic techniques and described his own work in this field (ref. 19). He concludes that the overall properties of atmospheric cosmic rays can be predicted accurately on the basis of a purely nucleonic cascade as a result of which all secondaries are mediated by pion production. Nevertheless, there are still matters of precise detail to be settled. Theoretical calculations are not yet in complete agreement with each other or with experimental data. Figure 1 compares the calculated and measured neutron spectra by Armstrong et al. (ref. 20). They have used a Monte Carlo code to compute the production of protons, charged pions, and neutrons by the incident galactic protons, and the subsequent transport of these particles down to energies of 12 MeV. The production of neutrons of energy  $\leq 12$  MeV as calculated by the Monte Carlo code was used as input to a discrete-ordinate code to obtain the low-energy neutron spectrum. The calculated and measured

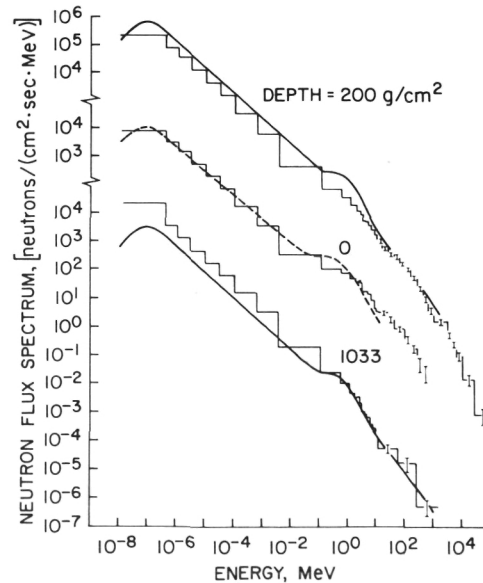


Figure 1.— Neutron flux spectra at various depths in the Earth's atmosphere, produced by galactic protons near solar minimum. Armstrong's calculations (histograms) are compared with those of Lingenfelder (dashed line) and the measurements of Hess et al. (solid line) for geomagnetic latitudes 40–44° (from Armstrong et al., ref. 20).

spectra differ somewhat at lower energies but are in good agreement at high energies. Merker (ref. 21), using a similar calculational technique, derived a spectrum that has a larger fraction of neutrons above 10 MeV than indicated by the experimental data of Hess et al. Merker's calculations show no evidence of an "evaporation bump" and, consequently, suggest that the fraction of total neutron dose equivalent due to neutrons above 10 MeV is greater than had been generally accepted. For example, Merker calculates that, at altitudes below 17 km, about 46 percent of the neutron dose equivalent results from neutrons having energies greater than 10 MeV, compared with Patterson's earlier estimate of 18 percent.

Thus, at the present time, both experimental measurements and theoretical calculations are insufficiently accurate. In an attempt to resolve these discrepancies, Ames Research Center, Brookhaven National Laboratory, Lawrence Berkeley and Lawrence Livermore Laboratories of the University of California, and the Physics Department of San Jose State University cooperated in a series of measurements made at high altitudes, approximately 12.5 km (41,000 ft), of the flux and spectrum of cosmic-ray neutrons. It is appropriate that new measurements be undertaken at the present time because great improvements in neutron detection techniques and spectrum-unfolding programs (ref. 22) have been made since the work of Hess et al. in 1959. Furthermore, over the past 10 years, the conversion of neutron spectra to dose equivalent has become better understood.

The specific goals of the Ames Research Center collaborative study include

1. The atmospheric neutron spectrum will be determined with greater accuracy than before, especially in the region from 1 to 100 MeV. The magnitude of the evaporation bump around 1 MeV suggested by Hess et al. will be determined and the region between 10 and 100 MeV will be examined to determine whether the plateau predicted by Merker exists. The spectral shape in the thermal, epithermal, and intermediate energy regions will be investigated using Bonner spheres. The region above 1 MeV will be investigated principally with the aid of activation threshold detectors.

2. Absolute neutron intensity measurements will be made as a function of altitude and geomagnetic latitude over an extended period to determine the influence of solar activity.

3. A solar-flare neutron dosimetry package will be developed which may be rapidly taken to high altitude during a solar flare. The influence of solar flares on the atmospheric neutron spectrum at aircraft altitudes has not yet been adequately measured, largely because of the long lead time necessary to assemble active neutron detectors following the onset of a solar flare. It is hoped that passive activation detectors may prove convenient for this purpose.

If these goals are achieved, the data obtained will have several important applications:

1. Cascade processes: Measurements of neutron intensity and spectra are a sensitive test of the accuracy of theoretical calculations of cascade phenomena and therefore of our understanding of the fundamental physical processes.

2. Cosmogenic radionuclide production: The cosmogenically produced radionuclides such as  $^3\text{H}$ ,  $^7\text{Be}$ ,  $^{14}\text{C}$ ,  $^{22}\text{Na}$ , and  $^{41}\text{Ar}$  result from the interactions of cosmic rays with the atmosphere. An improved understanding of cosmic-ray interactions will therefore improve our understanding of the production of these radionuclides.

3. Van Allen radiation belts: Neutrons produced near the top of the atmosphere may leak outward from the Earth, decay to protons, and be captured in the inner Van Allen radiation belt. It has been suggested that the production of neutrons in the upper atmosphere is sufficiently great to provide all the trapped protons observed in the belt. This is still an area of some controversy and reliable spectrum and intensity measurements will aid in its resolution.

4. Solar neutrons and solar flares: The development of reliable neutron detection systems will facilitate the detection of solar neutrons and the study of solar-flare phenomena. Detectors may be taken aboard the space shuttle for such research purposes.

5. Radiation exposure to man: Improved estimates of the radiation exposure to man due to cosmic rays both at altitude and on the ground will result from the work.

This report describes the progress to date of the collaborative study group during its first year of work. It mainly describes the development of experimental equipment although some preliminary data and tentative conclusions are discussed. During the period reported, neutron detectors were carried aboard three flights primarily to test the feasibility of several detection systems for reliability and sensitivity. The first two flights were devoted primarily to astronomical experimental flights with the cosmic-ray neutron measurements as auxiliary experiments. A portion of the third flight was flown along a constant geomagnetic parallel, one of the primary requirements for obtaining reliable cosmic-ray data.

The authors express their gratitude to Dr. Hans Mark, Director, Ames Research Center and to Mr. C. A. Syvertson, Deputy Director, Ames Research Center, for their interest and assistance in this work. Thanks are also due Dr. E. L. Chupp, University of New Hampshire; Dr. R. W. Wallace, Lawrence Berkeley Laboratory; Dr. W. M. Hess, Director of Environmental Research Laboratories, Dept. of Commerce and Dr. J. McLaughlin and Dr. F. Hajnal of the Health and Safety Laboratory, ERDA, New York, for providing useful information and encouragement. Dr. A. Tucker, San Jose State University, served as a consultant for our use of the liquid scintillation detector and assisted in interpreting the flight data. Dr. R. Mendell, New York University, and Dr. John Wilson, Langley Research Center, helped us to acquire this detector and provided invaluable background information about its history and development. G. K. Kojima, Ames Research Center, aided in analyzing and modifying the electronic circuitry of the system. Professor J. T. Routti, Helsinki University of Technology, gave advice concerning the LOUHI unfolding routine. Dr. Dennis Slaughter, Lawrence Livermore Laboratory, assisted in neutron calibrations. R. M. Cameron and C. M. Gillespie, Jr., Ames Research Center, were extremely helpful in arranging for flight time and locating the experimental equipment on the C-141 aircraft. This work was supported in part by the U.S. Energy Research and Development Administration.

## EXPERIMENTAL TECHNIQUES

### Description of Aircraft

The NASA C-141 Airborne Infrared Observatory (Airo) is a national facility dedicated to research in astronomy (fig. 2). The observing platform is modified Lockheed C-141 aircraft with a range of 9700 km (6000 mi.) and an operating ceiling of approximately 13.7 km (45,000 ft). The telescope, a conventional Cassegrain with a 91.5-cm open aperture, is designed primarily for observation in the 1 to 2000  $\mu\text{m}$  spectral region (ref. 23). A removable hatch permits open-port observations between elevations of  $35^\circ$  and  $75^\circ$ . Westward flying permits several hours of observation of an object near transit at constant bearing (azimuth) with little change in elevation. The telescope and its associated computerized control system occupy the center section of the aircraft (fig. 3). Typical experiments being flown on the Airo involve photometry of the gas and dust clouds found in interstellar space, in other galaxies, and in the center of our own, and also spectroscopy of the major planets. Auxiliary measurements of atmospheric constituents include water vapor determinations and infrared spectrograms of atmospheric molecules, such as  $\text{H}_2\text{O}$ ,  $\text{NO}_2$ , and  $\text{CO}_2$ . Of particular interest is a recent flight on which the principal investigator, Dr. H. Larson of the University of Arizona, made spectroscopic observations of Jupiter in the 1 to 6  $\mu\text{m}$  spectral region. Water vapor was observed deep in the Jovian atmosphere for the first time on this flight.

On the three flights described here, the neutron and charged particle instrumentation was located in the rear of the aircraft. The Bonner spheres were mounted on the aft cargo door (fig. 4).



Figure 2.— Ames C-141 Airborne Infrared Observatory; telescope hatch shown in open position.

A series of flights is planned at regular intervals over a significant portion of the solar cycle. Several types of aircraft are available at Ames, including the C-141, the Lear Jet, and the CV-990. All of these aircraft operate between 12.2 km (40,000 ft) and 13.7 km (45,000 ft). A U-2, which operates at 19.8 km (65,000 ft) with a restricted load capability may also be used.

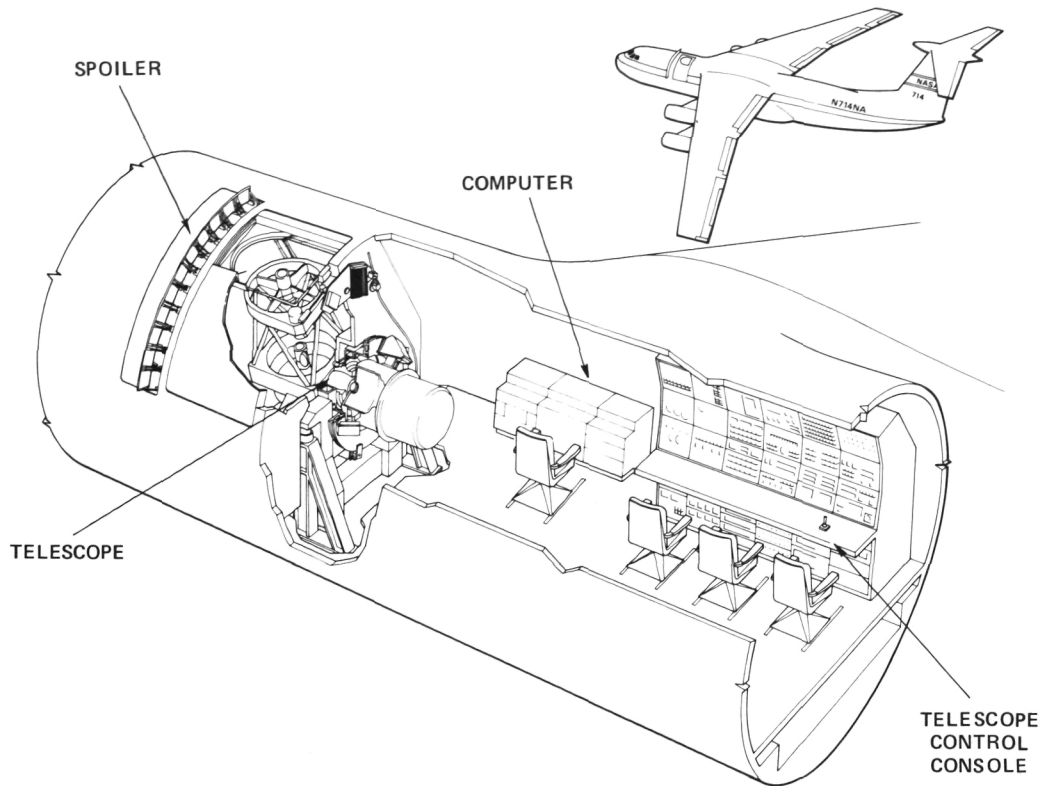


Figure 3.— Center section of the C-141 showing the location of the telescope and computerized control console.

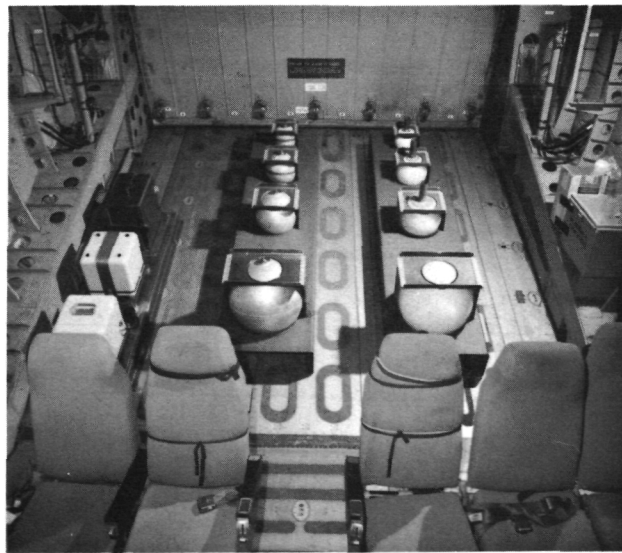


Figure 4.— View of aft loading area of C-141 aircraft. The Reuter-Stokes (RSS-111) ionization chamber and Brookhaven National Laboratory dose equivalent meter (DEM) are mounted on the left. Two sets of Bonner sphere moderators are mounted on the cargo door.

## Radiation Detectors

*Bonner spheres*— Two sets of spherical moderators (Bonner spheres, see ref. 24) are used to determine the shape of the neutron spectrum, principally in the energy region from thermal to about 20 MeV. The moderating spheres, varying in size from 5.1 cm (2 in.) to 45.7 cm (18 in.) in diameter (table 2), were made either of polyethylene or a water-filled aluminum shell (fig. 5).

TABLE 2.— SPHERICAL MODERATORS

Sphere diameter, cm	Moderator	
	<sup>6</sup> Li I crystal detector	Fission foil detectors
5.1 cm (2 in.)	Polyethylene	Polyethylene
7.6 cm (3 in.)	Polyethylene	Polyethylene
12.7 cm (5 in.)	Polyethylene	Polyethylene
20.3 cm (8 in.)	Polyethylene	Water
25.4 cm (10 in.)	Polyethylene	Water
30.5 cm (12 in.)	Polyethylene	Water
45.7 cm (18 in.)	Polyethylene	Water



Figure 5.— Detailed view of the Bonner sphere moderators: water-filled aluminum shells on left and polyethylene spheres on right. Guide tubes for the LiI detector may be seen on three polyethylene spheres.

Thermal neutrons at the center of each moderator were measured either by passive <sup>235</sup>U fission track registration detectors (ref.25) or by a <sup>6</sup>LiI scintillator.

Each uranium fission track detector consisted of an 8- $\mu$ -thick sheet of polycarbonate plastic sandwiched between two 0.0025-cm-thick sheets of <sup>235</sup>U. After chemical etching, the fission-track density was determined by a spark-counting technique. The area of the fission foil used in these measurements was 5.7 cm<sup>2</sup> and the efficiency of detection approximately 0.3 spark counts/fission fragment. Since the fission foils are passive detectors and are analyzed after the aircraft flight, they were placed at the center of the moderators at takeoff and remained in position for the entire flight. Although the sensitivity of the track detectors is not high, it is adequate to give moderate precision (better than  $\pm 6$  percent) during a 4-hr flight at an altitude of 12.2 km (40,000 ft) for moder-

ators 5.1 cm (2 in.) to 30.5 cm (12 in.) in diameter. Statistical precision may be improved by carrying the detectors aboard several flights. The accumulation of background events on the ground may be prevented by separating the uranium foil from the plastic sheet. Because of the low sensitivity of the foils, relative to <sup>6</sup>LiI, and because of the lack of response functions for these detectors, they were not used to derive a neutron spectrum.

The  ${}^6\text{LiI}$  scintillator used was cylindrical, 1.27 cm in diameter and 1.27 cm high. Figure 6 shows a typical spectrum recorded on a 256-channel pulse height analyzer. The thermal neutron flux density is determined by integrating the counts observed under the  ${}^6\text{Li}(n,\alpha){}^3\text{H}$  peak and subtracting the counts due to the photon and charged-particle continuum (fig. 6). Counts were taken with the detector at the centers of all seven polyethylene moderators, as well as with both a bare and a cadmium-covered detector. The sensitivity of the detector-moderator system is sufficient to obtain a statistical precision of about  $\pm 1$  percent for each of nine measurements during a 4-hr flight at an altitude of 12.2 km (40,000 ft). With only one detector and pulse height analyzer, counts are accumulated with the moderators at different times. To correct for small changes in counting rate variations, the observed moderator counting rate may be normalized using a standard moderated  $\text{BF}_3$  counter (see section entitled “Moderated  $\text{BF}_3$  Proportional Counter”).

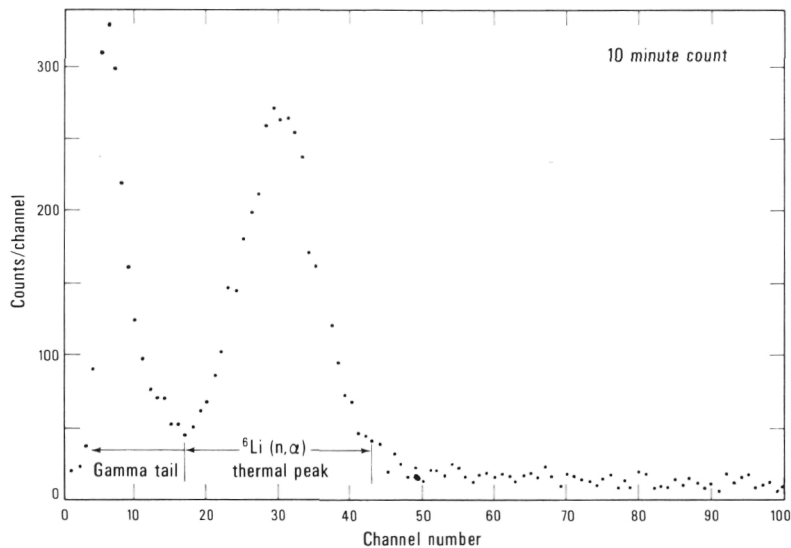


Figure 6.— Typical pulse height spectrum obtained from a 12.7-cm Bonner sphere at an altitude of 12.5 km (41,000 ft). The peak results from the  ${}^6\text{Li}(n,\alpha)$  reaction in the  $\text{LiI}$  detector.

Bonner-sphere response functions: From the measured Bonner-sphere responses in a neutron radiation field, the neutron spectrum may be derived if the response of each moderator is known as a function of energy. These response functions have been calculated over a wide range of energy, but empirical verification is limited and, in any event, does not extend above 15 MeV. No systematic studies of the 45.7-cm (18-in.) diameter moderator have been reported to date.

Figure 7 shows the response functions calculated by Sanna (ref. 26). The average responses over 31 energy intervals in the energy range from 0.5 eV to 400 MeV are plotted at the geometric mean of the energy range and a smooth curve is drawn through the points. The response functions of the 12.7-cm (5-in.) and 20.3-cm (8-in.) diameter moderators are seen to be incompatible with that used for the 15.2-cm (6-in.) diameter cylindrical moderator by the LBL group — particularly at energies above 15 MeV where no experimental data are available. It will therefore be an important part of this collaboration to systematically study the moderator responses as a function of energy using isotropic neutron sources and essentially monoenergetic neutrons from accelerators, for example, the Cyclograph (0.02-20 MeV) and ICT neutron generator (2.2 and 14 MeV) at Livermore and the 184-in. synchrocyclotron (220 MeV) at Berkeley.

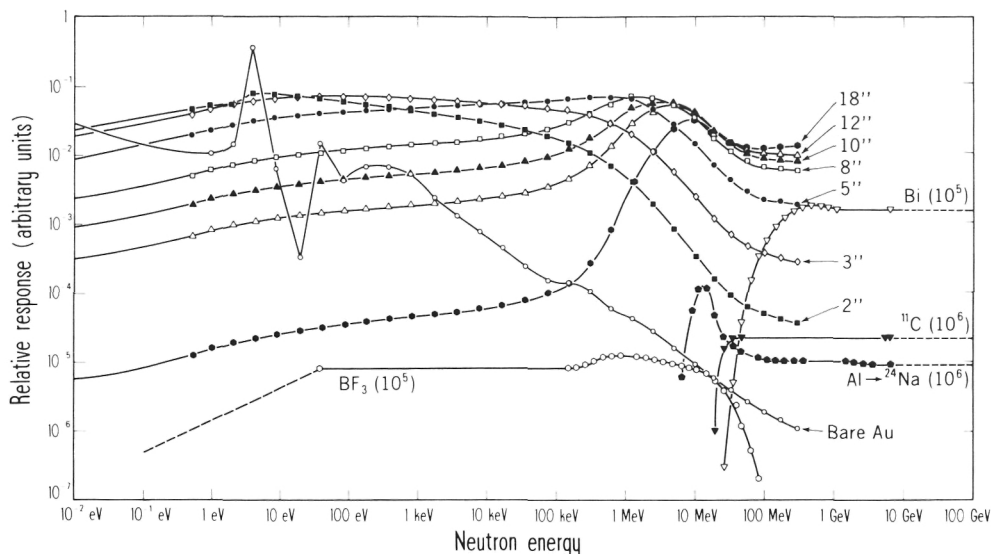


Figure 7.— Response of Bonner sphere moderators and activation detectors as a function of neutron energy.

*Activation detectors*— The following detectors have been flown on the flights to date: moderated gold foils, aluminum disks, sodium carbonate ( $\text{Na}_2\text{CO}_3$ ), and moderated manganese metal.

Table 3 lists the detectors and some of their characteristics.

TABLE 3. ACTIVATION DETECTORS CHARACTERISTICS

Detector	Isotope	T 1/2(min)	Bkg(cpm) <sup>a</sup>	% $A_s$ after 4-hr exposure <sup>b</sup>	Sensitivity <sup>c</sup>
1. Moderated gold foil 5.1 cm (2 in.) $\times$ 0.002 in.	$^{198}\text{Au}$	3888	34	4.188	69.4
2. Al Discs 20.3 cm (8 in.) $\times$ 1 in.	$^{24}\text{Na}$	897	71	16.93	
3. $\text{Na}_2\text{CO}_3$ (870g) $\times$ 2.5 cm (1 in.)	$^{24}\text{Na}$	897	70	16.93	83.0
4. Moderated Mn metal (100 g sample)	$^{56}\text{Mn}$	155.2	52.6	15.76	174.0

<sup>a</sup> Determined in same energy channels and same mass of unirradiated material.

<sup>b</sup>  $A_s$ : Activity at saturation after an infinite exposure time.

<sup>c</sup> Sensitivity: Counts per minute per unit neutron flux density from  $^{238}\text{PuBe}$  ( $\alpha, n$ ) source #632. National Bureau of Standards calibrated at  $7.90 \times 10^7$  n/sec. Counts taken immediately following irradiation.

**Moderated gold:** The gold foils used here were carried inside standard LBL paraffin-filled cadmium covered moderators (ref. 27). The moderators are right circular cylinders 15 cm in diameter by 15 cm in height. The energy response of these detectors is nearly flat for neutrons in the energy range from 0.02 to 20 MeV. Five foils are counted together on a 12.7-cm (5-in.) diameter NaI gamma scintillation detector. As many as 10 foils can be counted together with some improvement in overall statistics.

**Aluminum disks:** Aluminum disks were used on all flights. The reaction,  $^{27}\text{Al} (n, \alpha) ^{24}\text{Na}$ , has been used as a method for fast neutron detection for many years.  $^{24}\text{Na}$  has a favorable half-life of

15 hr and two energetic gamma rays in high abundance (1.37 and 2.74 MeV each at 100 percent per decay). Several disks can be counted on a single crystal detector due to the relative transparency of Al to these gamma rays.

A single disk, 20.3 cm (8 in.) in diameter by 2.5 cm (1 in.) thick, has a sensitivity to 14 MeV neutrons of 65 cpm when counted immediately after irradiation to equilibrium, while a stack of three 25.4 cm (10-in.) diameter by 2.5 cm (1-in.) thick disks counted together has a sensitivity of 160 cpm for the same energy range. The background increases from 71 to 73 cpm because of the presence of a few parts per million of  $^{232}\text{Th}$  decay-chain radionuclides in the aluminum.

The response function (cross section vs. neutron energy curve) used for the  $^{27}\text{Al}(n, \alpha)^{24}\text{Na}$  reaction is a blend of neutron data for energies below 20 MeV with proton data for all higher energies. No reliable neutron data exist for energies above 20 MeV. The two kinds of data are joined with a smooth curve which ignores any resonance peaks that may exist in the proton data. It is assumed that the neutron cross-sectional values are equal to the proton values throughout the energy range for which only proton data exist.

The aluminum detector was calibrated at 14 MeV neutron energy using the (d, t) reaction at a Cockcroft-Walton-type accelerator in which the absolute neutron yield was determined with an associated particle counter. The neutron yield was known to  $\pm 2$  percent absolute; statistical errors of counting data from the calibration exposures were kept well below this value, so the calibration results should be as accurate as the yield determination.

Sodium carbonate thermal neutron detector: Two 15.2-cm (6-in.) diameter by 3.8 cm (1.5 in.) thick plastic containers each with 870 gm of  $\text{Na}_2\text{CO}_3$ , were used as thermal neutron detectors. The samples flown on the second and third flights were of sufficient activity to be counted with a reasonable statistical accuracy ( $\pm 1$  percent).

Moderated manganese metal: Moderated manganese metal has been used on two flights and can provide a fast neutron detector with a high sensitivity. This detector can be used as an independent monitor for comparison with the active  $\text{BF}_3$  detector, chosen as the primary monitor.

*Moderated  $\text{BF}_3$  proportional counter*—  $\text{BF}_3$  proportional counters are widely used as neutron detectors (ref. 28). The counter used in this experiment is 5.1 cm in diameter by 22.9 cm active length. It is filled with 96 percent enriched  $^{10}\text{B}$  to 20 cm Hg. A 6.4-cm-thick paraffin moderator surrounded by 0.8-mm (0.03-in.) cadmium is used as the jacket for the  $\text{BF}_3$  counter and provides a reasonably flat response to 0.02- to 20-MeV neutrons (fig. 8).

*Brookhaven National Laboratory dose equivalent meter (DEM)*— The Brookhaven dose equivalent meter (refs. 29–31), a Rossi-type LET spectrometer (ref. 32) with a modified electrode system designed by Benjamin et al. (ref. 33), is used as a portable, mixed-radiation dose equivalent meter (DEM) (fig. 4). The detector consists of a 0.6-cm-thick spherical shell approximately 20 cm in diameter constructed of A-150 Shonka conducting plastic. The spectrometer gas filling consists of the usual "tissue equivalent" mixture of 66 percent methane, 3 percent nitrogen, and 31 percent carbon dioxide at a pressure of 10 torr. Under these conditions, the detector simulates a tissue sphere approximately 3  $\mu$  in diameter.

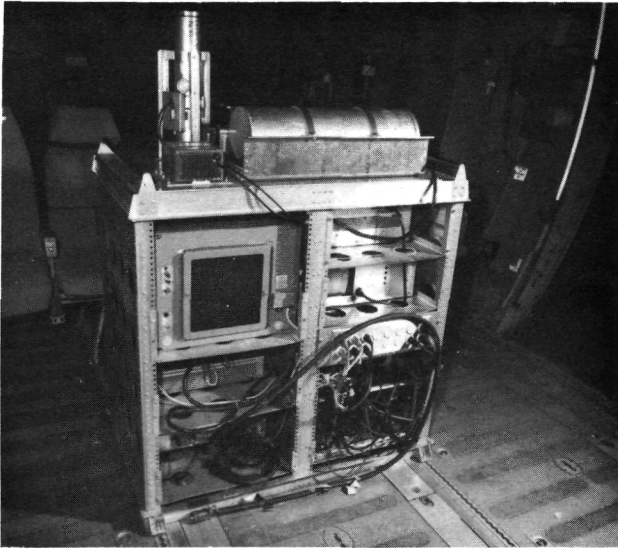


Figure 8.— View of the moderated  $\text{BF}_3$  and liquid scintillation detectors and associated electronics. The detectors are mounted on top of an aircraft rack. The  $\text{BF}_3$  counter (to the right) is lying horizontally and the liquid scintillation detector (to the left) is mounted vertically.

Since particles may traverse any chord of the sphere from a diameter to a line “grazing” the gas volume, particles of constant linear energy transfer values ( $L$ ) produce a variety of pulse sizes. The spectrum obtained from a radiation field can be considered to be composed of a summation of approximately triangular spectra, each due to particles with a given  $L$  value. The  $L$  values can range from approximately  $0.2 \text{ keV}/\mu$  at minimum ionization to  $1000 \text{ keV}/\mu$  for a heavy ion.

The absorbed dose can be measured by summing up the total energy deposited but the problem of determining the dose equivalent is more difficult. The usual method would be to obtain the particle number vs.  $L$  spectrum and multiply each value of  $L$  by a quality factor  $Q$  to account for the different biological effects produced by particles of different  $L$  values. The DEM derives the dose equivalent electronically. It contains a gain function that amplifies the pulse from an incoming particle in proportion to the  $Q$  value of the particle.

An ionizing event in the detector produces a current pulse that is converted to a voltage pulse proportional to the initial event and then is modified by two special biased amplifier systems to produce an output proportional to the dose equivalent rate. This electronic conversion obviates the need for laborious data reduction of the event-size spectra to yield the dose equivalent and allows one to construct a portable instrument for routine application. Because both the observed dose rate and the dose equivalent rate are presented, the average quality factor may also be determined.

The instrument flown was equipped with mechanical registers that printed accumulated  $\mu\text{rad}$  and  $\mu\text{rem}$  every 2 min. The detector was calibrated about an hour before and immediately following each flight with an internal alpha source that had been previously calibrated against a radium standard. Small changes ( $<10$  percent) in sensitivity due to temperature variations during the flight were corrected by using the preflight and postflight calibration data and assuming a linear variation between the two.

*Reuter Stokes RSS-111 environmental radiation monitor*— The RSS-111 is a sensitive gamma exposure monitoring system designed to measure and record low-level exposure rates such as those due to fallout and natural background radiation at ground level (ref. 34) (fig. 4). To measure the higher exposure levels at aircraft altitudes, the instrument was modified by the manufacturer to extend its range to  $1000 \mu\text{R}/\text{hr}$ .

The ionization chamber is spherical with a 25.4 cm (10 in.) diameter, a sensitive volume of 8 liters, and a wall thickness of 3 mm (0.12 in.) of stainless steel. The fill gas is pure argon at a pressure of 25 atm at  $0^\circ \text{C}$ .

When radiation is incident upon the chamber ion pairs produced in the active volume are swept to the electrodes by a collecting potential. The resulting current is measured by an electrometer and can be related directly to the free air ionization rate. The total measured ionization may be expressed as

$$R_t = R_\gamma + R_c + R_\alpha$$

where  $R_c$  represents the cosmic radiation response;  $R_\gamma$ , the gamma ray response, and  $R_\alpha$ , a component due to the alpha activity inherent in the stainless steel.

In the absence of a source of gamma rays other than those that are part of the cosmic radiation,

$$R_t = R_c \text{ (amp)} = k_c I_c$$

where  $I_c = \mu R/\text{hr}$  and  $k_c = 30.4 \times 10^{-15}$  amp/ $\mu R/\text{hr}$ . For example, at an atmospheric pressure of 1033 g/cm<sup>2</sup>, a mean level of  $I_c$  valid for the continental United States is 3.6  $\mu R/\text{hr}$ .

The RSS-111 was calibrated at the factory using a Co-60 source calibrated by the National Bureau of Standards. The "shadow shield" method was used to determine the fraction of each reading which resulted from scattered radiation. This quantity was then subtracted to obtain that portion of the reading due to the primary radiation. The proportionality constant for Co-60 thus determined was then converted to a constant for the Ra-226 spectrum, which was used as the reference spectrum.

Another calibration was made using a Ra-226 source at the Stanford Linear Accelerator on July 2, 1974. On the 0 to 1000  $\mu R/\text{hr}$  scale, the results indicate that the chart recorder was 9 percent too high. However, no "shadow shield" was available. Previous work shows that typically 8 percent scattered radiation is expected during calibration runs. Subtracting this value from the Stanford result gives an estimated instrument error of 1 percent.

*Liquid scintillation detector*— The liquid scintillation detector (LSD) allows one to observe the cosmic-ray neutron spectrum in an energy "window" of precisely specified width not found in other instrumentation. The LSD "window" was set for 3-13 MeV during flight 3 in October 1974. The general shape of the spectrum in this energy region is thought to follow an inverse power law with respect to energy (ref. 46). The value for the power exponent, known as the spectral index, is insensitive to changes in altitude and latitude. Since the region of the neutron spectrum between 1 and 10 MeV contains the largest concentration of the induced fast neutrons, variations in the solar activity, which modulate the primary cosmic-ray flux will be readily observed by changes in the integral values of the neutron flux in this energy range. The above characteristics of LSD along with its relatively high efficiency ( $\approx 30$  percent), compact dimensions and light weight make this a valuable instrument in evolving a "package" that can detect solar-flare influence on atmospheric neutrons as well as monitor the progress and fix one's position in the solar cycle.

Basic principle: The liquid scintillation detector responds to recoil protons generated when neutrons collide with hydrogen of the scintillation material. The resulting recoil proton ionizes the

medium along its path with a consequent emission of light quanta. A photomultiplier, optically coupled to the scintillation material, amplifies the light output so that it may be further processed and analyzed electronically. The amplitude of the photomultiplier pulse taken from the eleventh dynode carries information representative of the energy imparted to the recoil proton. Signals from the anode and thirteenth dynode are used in a pulse shape analysis circuit to characterize the particle type and thus provide discrimination against gammas. This is possible because the time dependence of the pulse intensity is different for gammas and neutrons (ref. 35). The anode pulse is analyzed for its fast component while the slow component is found by examining the thirteenth dynode pulse. It is further necessary to distinguish between charged particles originating from neutron collisions with the scintillator material and those that enter from outside, such as cosmic-ray protons, mesons, or particles which may not be considered "electron-like" in terms of scintillation decay time. To accommodate the discrimination of those charged particles originating from outside the detector and which are not minimum ionizing, the central volume of scintillation material (NE-218) was contained in a cylindrical vessel of NE-102 plastic scintillator. This outer scintillator acts as an anticoincidence shield for charged particles. A charged particle traversing this shield produces a light pulse with decay time characteristics similar to those of a gamma-ray induced pulse in the NE-218 and thus is rejected by the discriminator circuit.

Electronics: Figure 9 is a block diagram of the system electronics for the LSD. The main body of the detector, which includes the phoswich, pulse shape discriminator (PSD), Amperex 56 AVP photomultiplier tube (PMT), and high-voltage supply had been sealed and potted for high-altitude balloon observations. This unit was developed, calibrated, and used by Mendell and Korff (ref. 36) to record cosmic-ray fast neutrons in the range of 2-10 MeV during the period 1968 to 1971. It was acquired, along with several other units, by Ames in May 1974. The original system in which the detector unit was used was limited to seven channels of energy information. For our flights, most of the original electronics was replaced by standard NIM electronics and other commercial equipment.

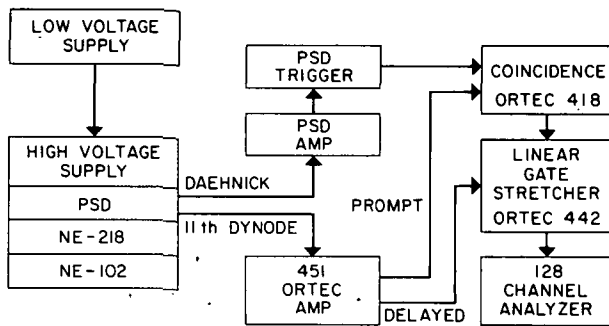


Figure 9.— Block diagram of the electronics used in conjunction with the liquid scintillation detector.

The PSD circuit is derived from one used by Daehnick and Sherr (ref. 37). It consists principally of two network branches that respond to the fast and slow components of a scintillation pulse. A negative signal proportional to the fast component (recoil electrons) of the scintillation pulse is obtained from the anode, differentiated, and then fed into a peak detector diode and pulse stretcher network which provides a signal of the desired rise and fall times. The slow component information is retrieved at the thirteenth dynode. A branch circuit integrates the pulse over a period long compared to that of the fast component. The resulting integrated positive signal is added to the fast negative signal to provide a net output, the sign and magnitude of which determines if the particle is a recoil proton or a minimum ionizing event, such as a Compton recoil electron.

The resultant PSD signal is amplified and received by a trigger circuit that sends a pulse to the coincidence unit when a neutron is detected. The linear signal from the eleventh dynode is amplified in the Ortec 451 unit and delivered to the coincidence module where the signal is delayed for

about 2  $\mu$ sec until the PSD trigger pulse arrives. The logic signal from the coincidence circuit opens the linear gate stretcher, allowing the amplified pulse from the 451 module to proceed to the 128-channel analyzer.

Calibration: The liquid scintillation device was tested at the Lawrence Livermore Laboratory, using the neutron generator of the Hazards Control Department. Pulse height distributions produced by 3- and 14-MeV neutrons were obtained. These neutrons were produced by  $^2\text{H}$  (d,n)  $^3\text{He}$  and  $^3\text{H}$  (d,n)  $^4\text{He}$  reactions, respectively.

Figure 10 shows the resulting recoil proton distribution produced by monoenergetic neutrons of approximately 14 MeV. A calibrated  $\text{BF}_3$  counter was used to monitor the neutron flux during each run. This allowed for a check on counts lost by electronics dead time and bias settings. From this information, a pulse height resolution of 40 percent was measured. This corresponds to about 30 percent in energy resolution because of the nonlinear relation between the pulse height ( $L$ ) and proton recoil energy ( $E_p$ ) which has the following approximate dependence  $L = 0.156 (E_p)^{1.5}$  for NE-213 (ref. 38). This should also apply to NE-218 used in this detector because of essentially the same variation of  $E_p$  with  $E_B$  where  $E_B$  is the beta energy (refs. 39 and 40).

The detector was used on the flight of October 22, 1974, in the configuration shown in figure 8. The system was operated and calibrated at one gain for the duration of the flight since the counting rate was too low to provide statistically meaningful geomagnetic data if gains were changed during the flight.

Preflight energy calibration was accomplished with Compton recoil electrons provided by two  $\gamma$ -ray sources,  $^{22}\text{Na}$  and  $^{137}\text{Cs}$ . If this information is to be used to measure proton energies, the relationships between the pulse heights produced by beta particles and recoil protons must be known. These relationships were provided by the work of Verbinski et al. (ref. 41). The half-height for the Compton edge of  $^{22}\text{Na}$  was taken as 1.12 MeV or 5 percent above the calculated value as prescribed by Flynn et al. (ref. 42).

Generally, the function relating pulse height to beta energy in organic scintillators for energies above 100 keV is given by the linear relation  $L = K (E_B - b)$ , where  $L$  is the relative pulse height,  $E_B$  the electron energy,  $K$  the slope for the system, and  $b$  the energy intercept ( $20 \pm 5$  keV) (ref. 42). With this information the gain of the system was calculated to be 0.063 MeV/channel.

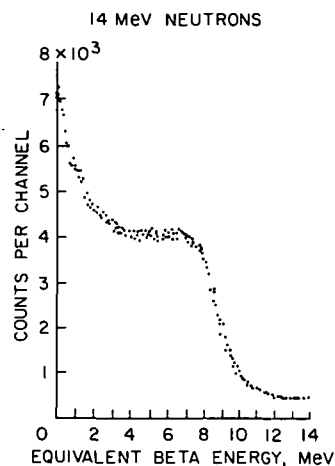


Figure 10.— Proton recoil spectrum obtained from the liquid scintillation detector.

## FLIGHT SUMMARY

Three data-taking flights have been made so far. The flights were made at night in the C-141 aircraft. The paths of each flight are plotted in figure 11 in geomagnetic coordinates. The basic information for each flight is summarized in this section.

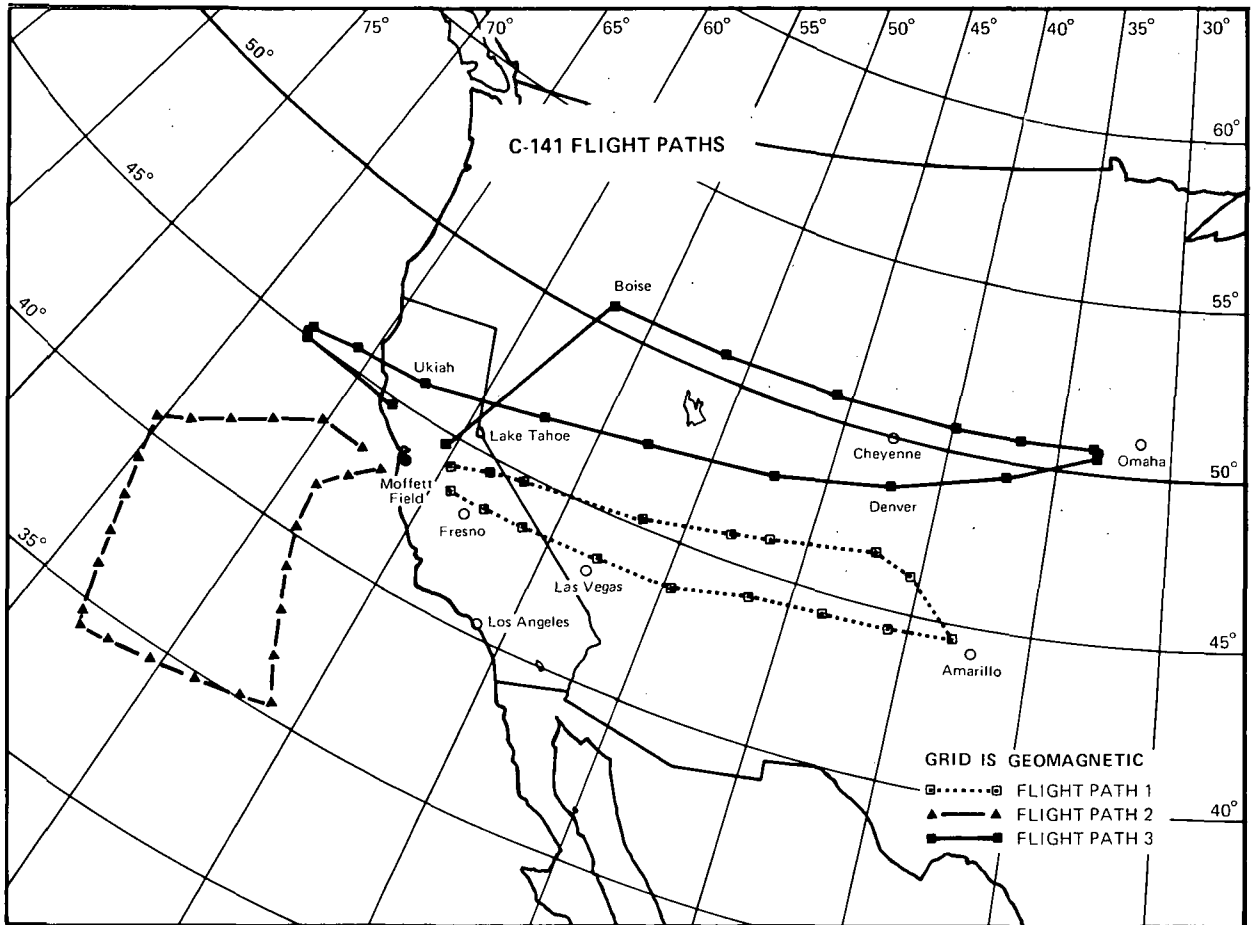


Figure 11.— Paths of the three C-141 flights described in this report; geomagnetic coordinates are shown.

### Flight 1 – 23-24 May 1974

This flight followed a path from Moffett Field to Amarillo, Texas ( $35^{\circ} 47'N$ ,  $101^{\circ} 39'W$ ). During the outward leg, the plane flew toward higher geomagnetic latitudes, roughly from  $\lambda = 43^{\circ}$  to  $47^{\circ}$  N. The flight pressure altitude was  $11.4$  km ( $37,400$  ft)  $\pm 0.03$  km (100 ft) for the initial quarter of the flight and  $12.8$  km ( $41,900$  ft)  $\pm 0.03$  km (100 ft) for the remainder. As indicated in the figure, the flight direction was approximately  $90^{\circ}$  on the outbound leg and  $270^{\circ}$  on the return leg. The total flight time was 5 hr and 15 min.

## Flight 2 – 5-6 June 1974

The path of this flight formed a rectangular pattern over the Pacific Ocean to the west of Ames Research Center. It began in a southwesterly direction, turned to the west, then to the north, and finally to the east. (The flight was terminated early because of a malfunction in the primary experimental equipment of the astronomers.) The altitude was quite constant, averaging 12.8 km (41,900 ft)  $\pm 0.03$  km (100 ft).

Following a flight path such as this caused rapid changes in geomagnetic latitude. The effect of this movement is clearly seen in the summary of the data. The total flight time was 4 hr and 20 min.

## Flight 3 – 22-23 October 1974

This flight was the first to follow a constant geomagnetic latitude path for a portion of the flight. It was ideal for the cosmic-ray neutron spectrum data recording. Arrangements were made for a leg of about 2 hr from Boise, Idaho, to Kearney, Nebraska, along the 50.7° N geomagnetic parallel of latitude (fig. 11); The flight time was 7 hr and 45 min. The flight altitude was 12.3 km (40,600 ft)  $\pm 0.03$  km (100 ft) pressure altitude.

Table 4 lists the instruments used and the flights on which they were flown. The first two flights were intended to determine if the sensitivity and reliability of all instruments were adequate. Data collected on these flights show the effect of changing geomagnetic latitude on the total neutron and charged-particle components. The third flight, flown along a constant geomagnetic latitude and therefore in a constant neutron flux, was the only flight so far in which sufficient data were collected to derive a cosmic-ray neutron spectrum and dose determination.

The data taken to date show that, for flights with a duration greater than 6 hr at altitude, good statistics are obtained from all detectors tested.

TABLE 4.— DETECTORS ON EACH FLIGHT

Number	Date (1974)	Bonner spheres		Al	Moderated BF <sub>3</sub> (monitor)	Ion chamber	Moderated Au foils	Moderated Mn metal	Dose equivalent meter	Liquid scintillation detector
		Active	Passive							
1	5/23-24	X	X	X	X	X	X		X	X
2	6/5-6	X	X	X	X	X	X	X	X	X
3	10/22-23	X	X	X	X	X	X	X	X	X

## ANALYSIS OF DATA

### BF<sub>3</sub> Neutron Detector and Reuter-Stokes Ionization Chamber Data

Figure 12 is a composite graph for flight 1. The RSS-111 chamber began operating before takeoff and continued until after the termination of the flight. The rapid increase in exposure rate

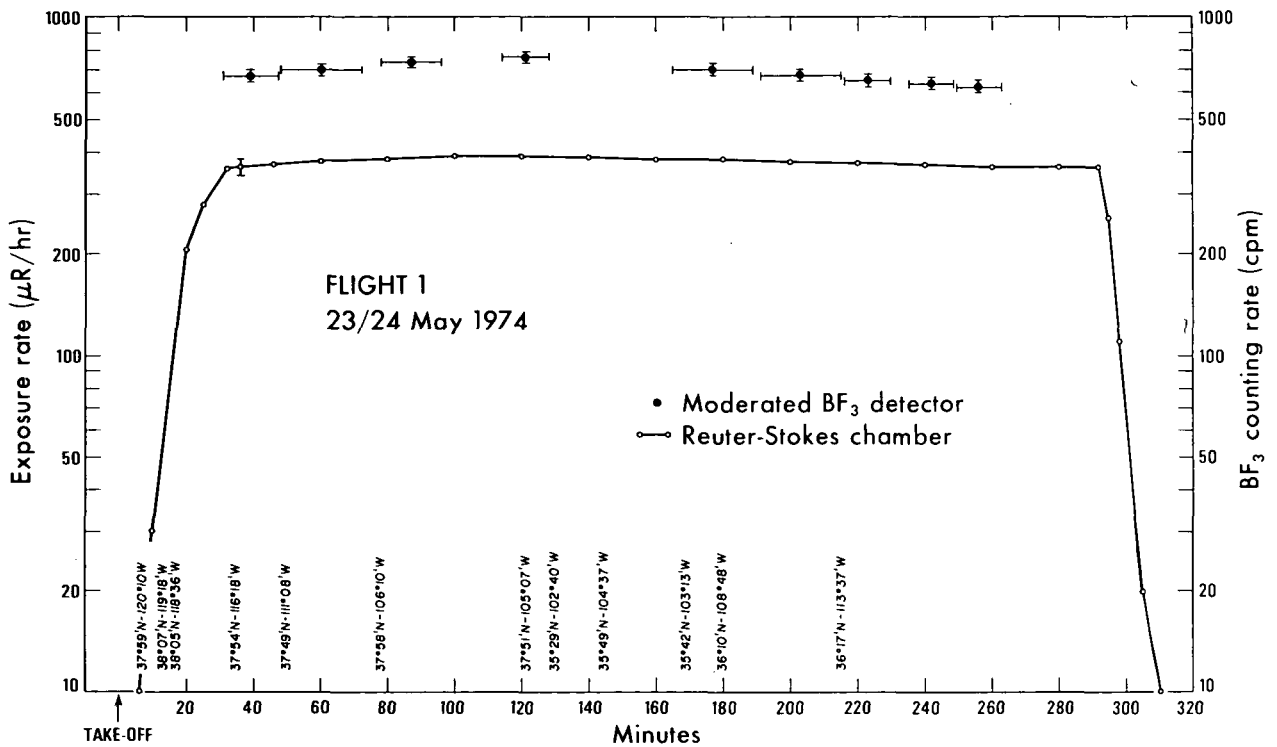


Figure 12.— A composite diagram showing experimental data taken on flight 1.

can be seen during the climb to flight altitude. When flight altitude was reached, the BF<sub>3</sub> neutron detector was started. Counting times varied in length, but the statistical accuracy was always better than 1 percent on every count.

Since this flight was made along a constant geographic latitude over the continental United States, the effect seen in all detectors used here is that of first moving to higher then lower geomagnetic latitudes. Because of its high sensitivity, it is clear that the moderated BF<sub>3</sub> detector can be very useful as an active monitor for all neutron-measuring instruments, and can provide the rate normalizing factors necessary for the interpretation of activation detector data.

Figure 13 is the composite for flight 2. As previously described, this flight was made in a southwesterly direction, moving to lower geomagnetic latitudes slowly, then a northward turn. The counting rate of the BF<sub>3</sub> neutron detector again proved to be a valuable reference during this flight.

Figure 14 is the composite for flight 3. A 2-hr portion of this flight was along the 51°N geomagnetic latitude. The flight was sufficiently long to allow good statistics for the Bonner sphere moderator set. Periods when measurements were made with the liquid scintillation detector are also indicated.

Several degrees of geomagnetic latitude were crossed on each flight. Since the minimum momentum required for a galactic proton to penetrate the Earth's magnetic field varies with the fourth power of the cosine of the geomagnetic latitude, the response of the ion chamber increased at higher latitudes. Figure 15 is a plot of the radiation exposure rate versus the geomagnetic latitude. The data are reasonably well fitted by a curve that shows the exposure rate as a constant

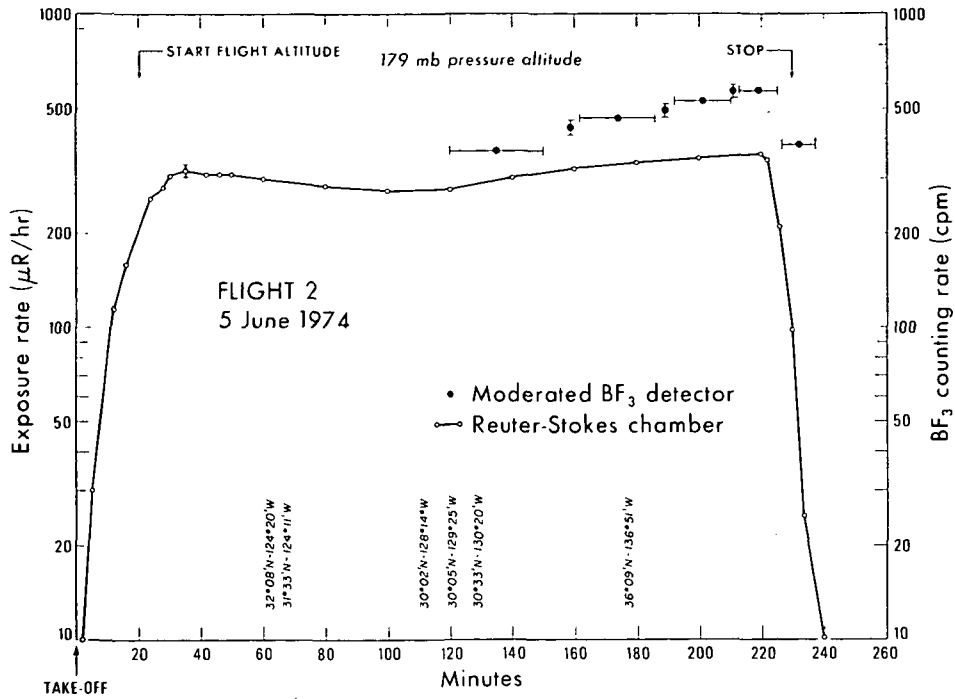


Figure 13.— A composite diagram showing experimental data taken on flight 2.

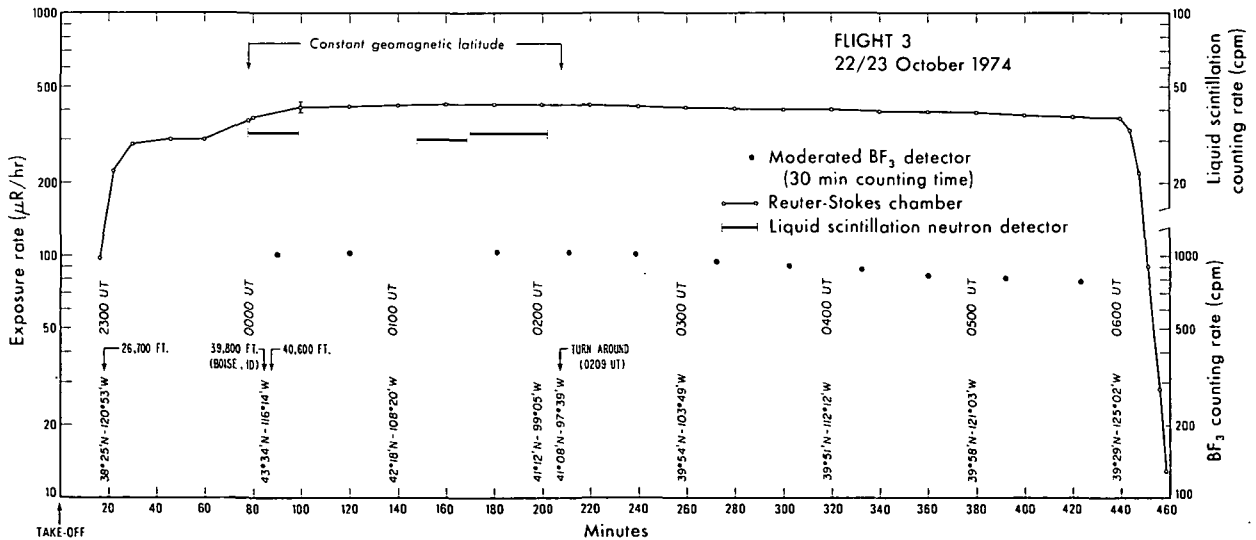


Figure 14.— A composite diagram showing experimental data taken on flight 3.

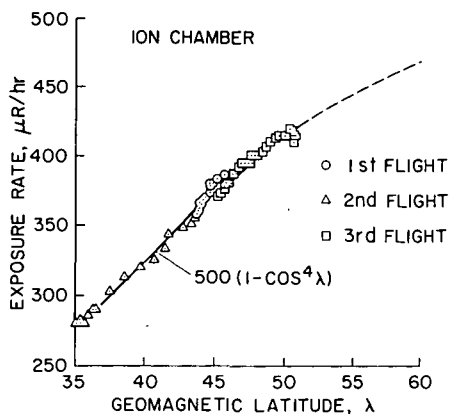


Figure 15.— Exposure rate measured by RSS-111 as a function of geomagnetic latitude for all flights.

times  $(1 - \cos^4 \lambda)$  where  $\lambda$  is the latitude in degrees. The approximate overall rate of change is  $10\mu R/\text{hr}/\text{deg}$ .

The changes in the neutron counts and the ion chamber counts with variations in geomagnetic latitude are illustrated in figure 16, where each type of measurement is plotted as a percentage of the reading at the beginning of the constant geomagnetic portion of flight 3. The figure indicates that the neutron flux is more sensitive to changes in latitude than is the total ionization produced by the charged particle and gamma fluxes.

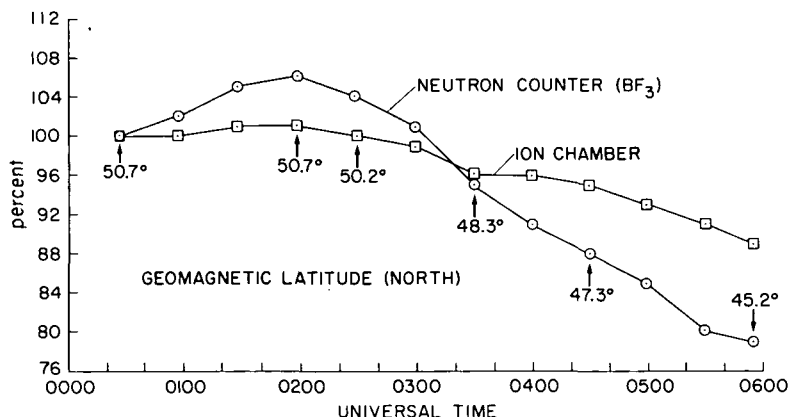


Figure 16.— Percent of ion chamber and moderated  $\text{BF}_3$  counter readings as a function of geomagnetic latitude.

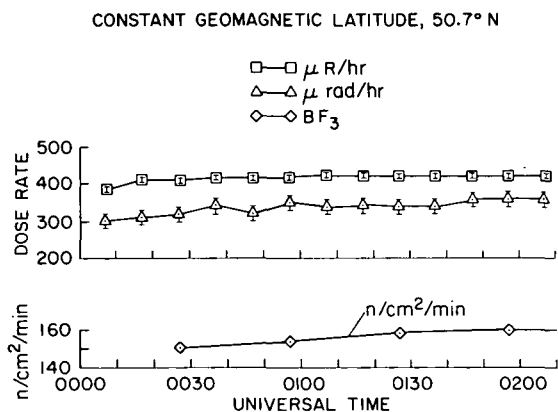


Figure 17.— Instrument readings plotted as a function of time on the constant geomagnetic leg of flight 3.

A 2-hr portion of the third flight was flown along a path of constant geomagnetic latitude. The instrument readings for this leg are plotted in figure 17. The ion chamber reading increased only slightly. Neutron counts from the  $\text{BF}_3$  counter are also shown. There is noticeable increase in their counting rate.

Figure 18 shows the decrease in ion chamber readings measured during descent, plotted against pressure altitude on a semilog plot. At 12.5 km (41,000 ft), the exposure rate was  $360\mu R/\text{hr}$  decreasing to  $6\mu R/\text{hr}$  at ground level. Between 3 km (10,000 ft) and 7.6 km (25,000 ft), the curve follows a straight line with a slope of 12.8 percent per 1000 ft. Using the standard atmosphere tables to convert the data to pressure, an "attenuation" coefficient of  $140\text{ g}/\text{cm}^2$  was obtained.

## Brookhaven National Laboratory Dose Equivalent Meter and Reuter-Stokes RS-111 Ionization Chamber Readings

The absorbed dose, dose equivalent, and exposure rates, as measured by the dose equivalent meter (DEM) and by the RSS-111 ion chamber, are presented for the three flights in figures 19 to 21. The time after takeoff is indicated on the abscissa. The latitude effect is clearly seen in the

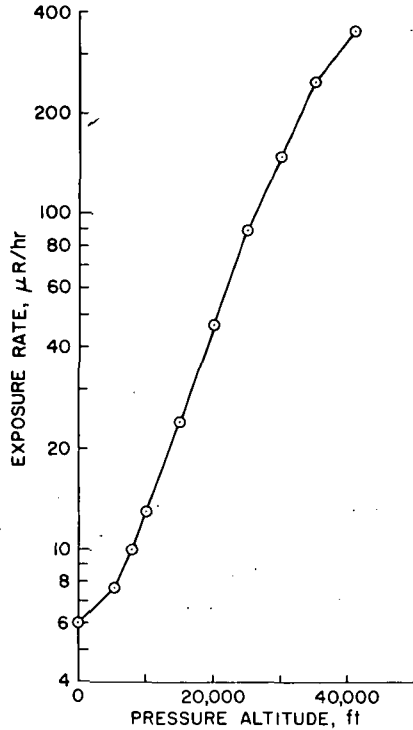


Figure 18.— Variations of RSS-111 ionization chamber readings with pressure altitude.

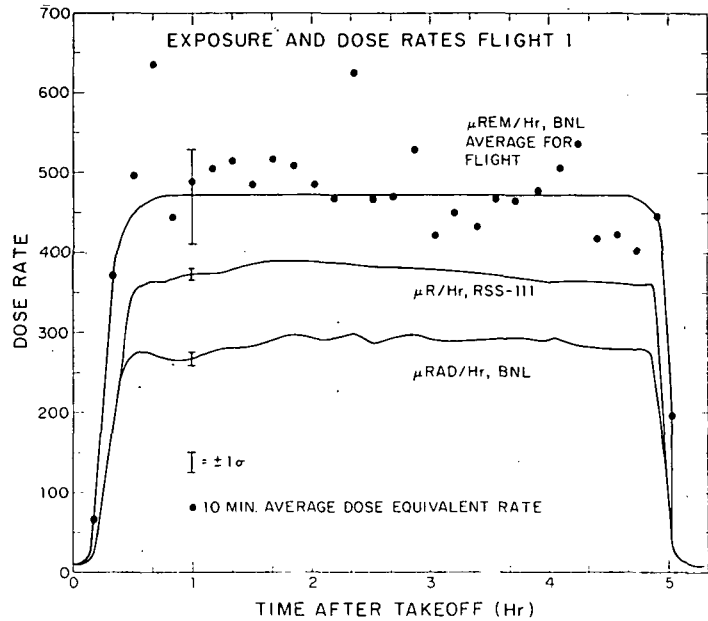


Figure 19.— Data contained from RSS-111 and DEM during flight 1.

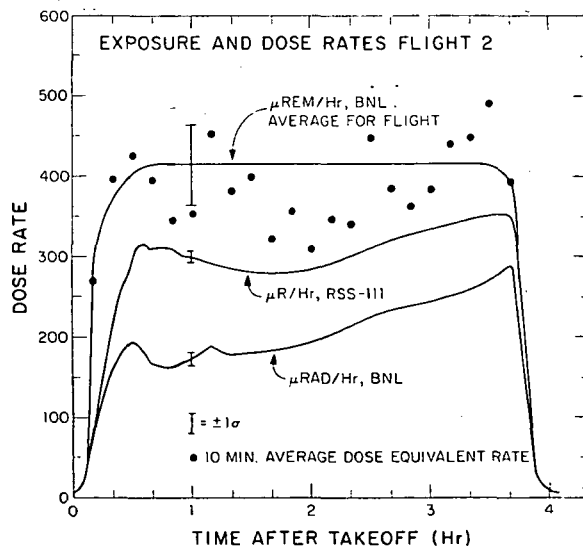


Figure 20.— Data obtained from RSS-111 and DEM during flight 2.

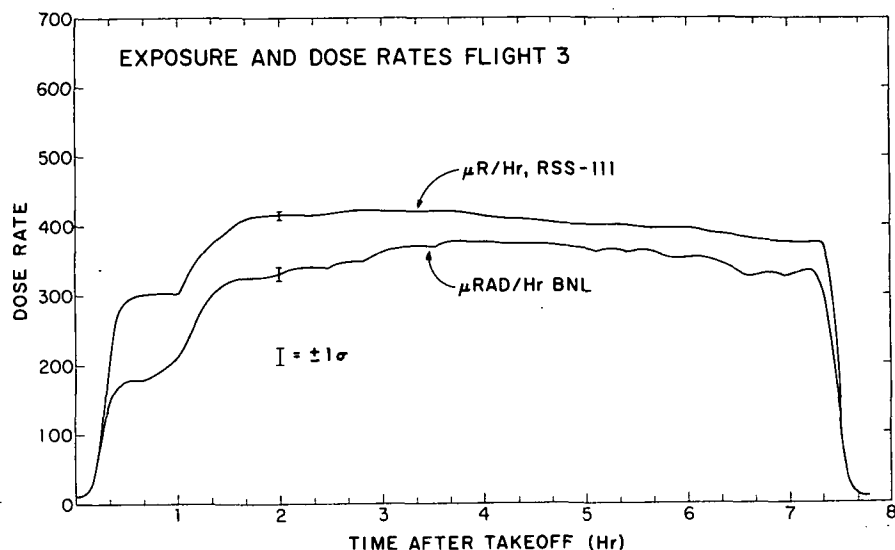


Figure 21.- Data obtained from RSS-111 and DEM during flight 3.

pronounced dip in both the exposure and absorbed dose rate measurements plotted for flight 2. The large variations in the dose equivalent rate observations for all flights are due to the electronic processing of the incoming radiation pulses and do not represent real variations in the dose equivalent rate of the radiation flux itself. The average values for each flight and the ratios between the measured quantities are given in table 5. No dose equivalent rate was measured for the third flight because one amplifier was not turned on. The average quality factor (QF) was determined by taking the ratio of the dose equivalent rate of the absorbed dose rate: 1.7 and 1.85 for the first and second flights, respectively.

TABLE 5.- AVERAGE EXPOSURE AND DOSE RATES

Flight no.	$\mu R/hr$	$\mu rad/hr$	$\mu rem/hr$	$\mu rad/\mu R$ ratio	$\mu rem/\mu rad$ ratio (quality factor)
1	374	276	468	0.74	1.70
2	311	226	418	.73	1.85
3	407	341	-	.84	-

The average QF is useful in estimating fractions of the absorbed dose and dose equivalent due to neutrons. If it is assumed that the measured radiation has a low LET component,  $L$ , consisting of photons, muons, and other charged particles with  $QF = 1$  and a neutron component,  $N$ , with  $QF = 6.5$  (ref. 43), one can write

$$QF_{(AVE)} = \frac{D_L(QF_L) + D_N(QF_N)}{D_L + D_N}$$

where  $D$  refers to the absorbed dose and  $D(QF)$  gives the dose equivalent. This equation can be rearranged to give

$$\frac{D_L}{D_N} = \frac{QF_N - QF_{AVE}}{QF_{AVE} - 1}$$

Using  $QF_{AVE} = 1.7$  from flight 1 and substituting 6.5 for  $QF_N$  yields

$$\frac{D_L}{D_N} = \frac{6.5 - 1.7}{1.7 - 1} = 7$$

The neutron component is therefore 12 percent of the total absorbed dose and 48 percent of the dose equivalent. These figures agree reasonably well with the calculations of O'Brien and McLaughlin (ref. 44) for a similar epoch, latitude, and altitude. Their values of 570 and 355 for the dose equivalent and absorbed dose rates, respectively, yield  $QF_{AVE} = 1.6$ . Substituting in the equation yields  $D_L = 8D_N$  and the neutron component in this case represents 11 percent of the absorbed dose and 45 percent of the dose equivalent.

#### Neutron Detector Data

Table 6 summarizes the data from the neutron activation detectors carried aboard flights 1 through 3. In addition, Bonner spheres were carried aboard all flights. A spectrum derived from the Bonner sphere data is presented in table 7.

Table 8 gives values of both average neutron flux density and average dose equivalent rate derived from these neutron measurements. In calculating dose equivalent rates, the following assumptions were made:

1. The moderated thermal neutron detectors, both active and passive, use the same thickness of moderator and therefore respond to the same energy region of the cosmic-ray neutron spectrum. This region corresponds to ~50 percent of the total neutron dose equivalent and the measured dose equivalent is therefore increased by a factor of 2 to give the values quoted in table 8 (ref. 18).

2. The dose equivalent rate quoted for the aluminum detector is obtained by combining the flux densities measured by the aluminum detector,  $\phi_{Al}$ , and by a moderated thermal neutron detector,  $\phi_{MOD}$ , such as  $BF_3$ , manganese metal, or gold, according to the empirical equation described by Gilbert et al. (ref. 28):

$$\text{Dose equivalent rate} = (0.35)(1.75) \left( \frac{\phi_{MOD}}{8.0} + \frac{\phi_{Al}}{3.3} \right)$$

For the Bonner sphere data, fluence to dose equivalent conversion factors from ICRP Publication 21 are used to calculate dose equivalent from the neutron spectrum given in table 7.

The neutron data obtained (table 8) are consistent and the calculated dose equivalent rates show good agreement for each flight.

TABLE 6.-- ACTIVATION DETECTOR DATA FOR FLIGHTS 1, 2, AND 3

Flight	Detector description	${}^aA_0$ c/min	${}^bA_s$ c/min	Counting standard deviation percent	c/min from unit flux density	BKG c/min	Flux density n/cm <sup>2</sup> -sec
1	Au foils (moderated)	7.3	155.0	±4	66	34.0	2.29
	Al disks (2 - 20.3 cm (8 in.) disks)	8.6	45.7	±5	100	70.2	0.46
	BF <sub>3</sub> counter (average rate)		690	1			1.70
2	Mn metal (200 g moderated)	230	384	±1	272	51.4	1.41
	Au foils (moderated)	3.8	107	±6	66	34.0	1.62
	Al disks (2 - 25.4 cm (10 in.) disks)	6.2	42.3	±5	132	72.8	0.32
	BF <sub>3</sub> counter (average rate)		446				1.09
3	Mn metal (800 g moderated)	740	899	±0.7	405	51.4	2.22
	Al disks (2 - 25.4 cm (10 in.) disks)	17.4	65.4	±2.8	132	72.0	0.495
	BF <sub>3</sub> counter (average rate)		927	1			2.28

${}^aA_0$  = initial activity at end of flight.

${}^bA_s$  = saturated activity if exposed to the cosmic-ray neutron flux for infinite time.

TABLE 7.- LOUHI CALCULATED SPECTRUM FROM BONNER SPHERE  
DATA OF FLIGHT 3

I	E(I), MeV	Differential flux, n/cm <sup>2</sup> /MeV	Integral flux, n/cm <sup>2</sup>	Integral dose equivalent, mrem/hr	Integral kerma, ergs/g/hr	Band width, MeV
1	2.07E-07	2.93E+07	1.00E+00	1.00E+00	1.00E+00	4.14E-07
2	5.32E-07	1.23E+07	9.36E-01	9.96E-01	1.00E+00	2.69E-07
3	9.93E-07	5.22E+06	9.18E-01	9.94E-01	1.00E+00	7.63E-07
4	2.10E-06	2.26E+06	8.97E-01	9.93E-01	1.00E+00	1.61E-06
5	4.45E-06	9.97E+05	8.78E-01	9.92E-01	1.00E+00	3.42E-06
6	9.42E-06	4.51E+05	8.60E-01	9.90E-01	1.00E+00	7.22E-06
7	2.00E-05	2.09E+05	8.42E-01	9.89E-01	1.00E+00	1.53E-05
8	4.22E-05	9.86E+04	8.25E-01	9.88E-01	1.00E+00	3.23E-05
9	8.94E-05	4.73E+04	8.08E-01	9.87E-01	1.00E+00	6.89E-05
10	1.89E-04	2.29E+04	7.91E-01	9.86E-01	1.00E+00	1.45E-04
11	4.04E-04	1.12E+04	7.74E-01	9.85E-01	1.00E+00	3.18E-04
12	8.55E-04	5.50E+03	7.55E-01	9.84E-01	9.99E-01	6.40E-04
13	1.80E-03	2.73E+03	7.36E-01	9.83E-01	9.99E-01	1.38E-03
14	3.80E-03	1.37E+03	7.16E-01	9.81E-01	9.99E-01	2.91E-03
15	8.05E-03	7.12E+02	6.95E-01	9.80E-01	9.99E-01	6.20E-03
16	1.70E-02	3.85E+02	6.71E-01	9.79E-01	9.98E-01	1.30E-02
17	3.61E-02	2.19E+02	6.45E-01	9.77E-01	9.95E-01	2.77E-02
18	7.64E-02	1.33E+02	6.13E-01	9.72E-01	9.90E-01	5.86E-02
19	1.58E-01	8.62E+01	5.71E-01	9.60E-01	9.77E-01	1.13E-01
20	3.18E-01	5.90E+01	5.20E-01	9.37E-01	9.50E-01	2.27E-01
21	6.40E-01	4.05E+01	4.49E-01	8.81E-01	8.96E-01	4.56E-01
22	1.29E+00	2.45E+01	3.51E-01	7.51E-01	7.87E-01	9.20E-01
23	2.59E+00	1.09E+01	2.31E-01	5.12E-01	5.97E-01	1.85E+00
24	5.22E+00	3.44E+00	1.24E-01	2.86E-01	3.78E-01	3.73E+00
25	1.05E+01	8.84E-01	5.57E-02	1.35E-01	1.98E-01	7.50E+00
26	1.96E+01	2.12E-01	2.05E-02	5.19E-02	7.76E-02	1.09E+01
27	3.40E+01	4.97E-02	8.20E-03	2.17E-02	3.11E-02	1.88E+01
28	5.87E+01	1.15E-02	3.24E-03	8.90E-03	1.23E-02	3.26E+01
29	1.02E+02	2.67E-03	1.24E-03	3.54E-03	4.71E-03	5.64E+01
30	1.76E+02	6.16E-04	4.46E-04	1.44E-03	1.69E-03	9.77E+01
31	3.04E+02	1.42E-04	1.27E-04	4.60E-04	4.81E-04	1.69E+02

Total flux = 1.8854E+02 n/cm<sup>2</sup>/min

Dose equivalent rate = 2.0036E-01 mrem/hr

45.7 cm (18 in.) sphere response is weighted 0.5

TABLE 8.— NEUTRON DOSE EQUIVALENT AND FLUX DENSITY

Flight	Detector <sup>a</sup>	Neutron flux density (n/cm <sup>2</sup> /sec)	Dose equivalent rate <sup>b</sup> (mrem/hr)
1	Au foil moderated	2.29	0.21
	Al disk	.46	.21
	BF <sub>3</sub> counter moderated (average count rate)	1.70	.16
2	Mn metal moderated	1.41	.13
	Au foil moderated	1.62	.15
	Al disks	.32	.14
	BF <sub>3</sub> counter moderated (average count rate)	1.09	.10
	Mn metal moderated	2.22	.20
3	Al disks	.495	.26
	BF <sub>3</sub> counter moderated (average count rate)	2.28	.21
	Bonner spheres	3.14	.20

<sup>a</sup>Moderated detectors measure 0 to 15 MeV neutrons, Al disks measure neutrons of energy greater than 6 MeV.

<sup>b</sup>For conversion of flux density to dose equivalent rate see section entitled "Neutron Detector Data."

## Neutron Spectrum Unfolding Computer Codes

*LOUHI*— To determine the neutron spectrum from the Bonner spheres and activation data, an unfolding code is used. A spectrum is assumed and the experimental data are compared to the data calculated for each detector from the spectrum and known detector response functions. The differences are then minimized.

To accomplish this, Routti (ref. 45) used a numerical technique (*LOUHI*) to solve first-order Fredholm integral equations incorporating a controlled degree of smoothness or closeness to a given approximate solution. A generalized formalism introduced by Routti is discussed below.

The integral equation

$$\int_{E_{min}}^{E_{max}} K(E', E) \phi(E) dE = A(E) + \epsilon(E') \quad (1)$$

where  $\epsilon(E')$  reflects the uncertainties and error and is first replaced by a quadrature form

$$K\phi = A + \epsilon \quad (2)$$

Here  $A$  is the measured spectrum with components  $A_j$  and errors  $\epsilon_j, j = 1, \dots, m$ ;  $\phi$  is the solution vector with components  $\phi_i, i = 1 \dots, n$ ; and  $K$  is the response matrix of dimensions  $n \times m$ . In the derivation of the quadrature form, the solution is approximated by a piecewise linear continuous function. With an adequate number of steps, this approximation provides an arbitrary closeness to any real continuous function without prescribing the shape of the solution.

The solution of the integral equation is obtained by minimizing the quadratic form

$$Q = Q_0 + \gamma (W_1 Q_1 + W_2 Q_2) \quad (3)$$

where

$$Q_0 = \sum_{j=1}^m r_j^\epsilon \epsilon_j^2$$

$$Q_1 = \sum_{i=1}^n r_i^{\phi^0} (\phi_i - \phi_i^0)^2$$

$$Q_2 = \sum_{i=2}^{n-1} r_i^d (\phi_{i-1} - 2\phi_i + \phi_{i+1})^2$$

The term  $Q_0$  is related to the matching of the responses, which can be weighted by  $r_j^\epsilon$ . The term  $Q_1$  requires closeness to a given approximate solution  $\phi^0$ ; this criterion may be weighted with an energy-dependent function specified by weights  $r_i^{\phi^0}$ . The term  $Q_2$  imposes a smoothness

requirement by including the numerical second derivative of the solution in the sum to be minimized; this also can be weighted with energy-dependent terms  $r_i^d$ .

The auxiliary conditions included in terms  $Q_1$  and  $Q_2$  are weighted relatively by  $W_1$  and  $W_2$ , and finally  $\gamma$  specifies the overall importance of the *a priori* conditions. The solution is obtained by minimizing  $Q$  with respect to  $\phi_i$  by setting

$$\frac{\partial Q}{\partial \phi_i} = 0 \text{ for } i = 1, \dots, n \quad (4)$$

The resulting equations can be written in matrix form and solved in a single matrix inversion.

However, the nonnegativity of the solution is not guaranteed. This leads to difficulties with large uncertainties in the measured responses and the cross sections, where a compromise must be made between matching the responses and satisfying the prior information. It is also difficult to properly weigh the auxiliary conditions when the neutron spectrum extends over many orders of magnitude.

*Generalized least-squares method with nonnegative solution*— To overcome the difficulties of the above matrix-inversion methods, Routti developed a formalism in which the solution is forced to be nonnegative and the auxiliary conditions can be used on several different scales. The neutron spectrum is again approximated by a piecewise linear continuous function defined at energy points  $E_i$  by intensity values  $\phi_i$ , which are taken to be squares of real numbers,  $\phi_i^2$ , to eliminate negative values. The requirements of matching the measured responses as well as satisfying the *a priori* conditions are combined by defining a quadratic form as in equation (3.) Because of computation-economy requirements, the neutron spectrum may be defined at fewer points than the cross sections. The constraints about the smoothness and approximate shape of the spectrum are now expressed either on a linear, a relative, or a logarithmic scale; for instance, on a logarithmic scale, as

$$\left. \begin{aligned} Q_1^{\log} &= \sum_{i=1}^n r_i (\log X_i^2 - \log \phi_i^0)^2 \\ Q_2^{\log} &= \sum_{i=2}^{n-1} r_i^d (\log X_{i-1}^2 - 2 \log X_i^2 - \log X_{i+1}^2)^2 \end{aligned} \right\} \quad (5)$$

The solution can no longer be obtained through matrix inversion, but rather by minimizing  $Q$  with respect to the parameters  $X_i$  through iterative techniques. A gradient minimization technique with variable metric was found to be well suited for this computation.

The formalism described above allows the combination of prior information of the neutron spectrum with the information contained in the measurement of the responses in a very flexible form. The method and the computer program LOUHI, written to perform the analysis, were subjected to mathematical tests. These results indicate that the method meets all the requirements set therein for a solution method. The technique is best suited for a large computer. In most cases, the solution obtained is not a sensitive function of the weighting parameters used in the expression of  $Q$ . However, when largely perturbed test responses or inconsistent sets of measured data are used,

the analysis benefits greatly from the possibility of running LOUHI on-line with cathode-ray-tube display on intermediate results and the option of choosing optimal weighting parameters while solving the problem.

*TUNS*— The pulse height spectra from the liquid scintillation detector (LSD) were unfolded by use of a computer code TUNS developed by Shook and Pierce of Lewis Research Center (ref. 39).

For monoenergetic neutrons, the number of recoil protons per unit energy per second,  $dN_p/dE_p$ , for an ideal scintillator excluding multiple scattering and wall effects is given as

$$\frac{dN_p}{dE_p} = A \epsilon \frac{\phi}{E_n} \quad (6)$$

where  $\phi$  is the incident neutron flux at energy  $E_n$ ,  $A$  is the area normal to the beam, and  $\epsilon$  is the efficiency of the scintillator. With a distribution of neutron energies, it is necessary to sum the contributions from each neutron of energy equal to or exceeding the value  $E_p$ .

The response is now given by an integral:

$$\frac{dN_p}{dE_p} = A \int_{E_n=E_p}^{\infty} \epsilon(E_n) \frac{\phi(E_n)}{E_n} dE_n \quad (7)$$

where  $\epsilon(E_n)$  is now a function of energy and  $\phi(E_n)$  is a differential neutron flux  $dF/dE_n$ . Solving for the differential neutron flux by differentiating each side of equation (7) with respect to  $E_p$  yields

$$\phi(E_n) = - \frac{E_n}{A\epsilon(E_n)} \left( \frac{d^2 N_p}{dE_p^2} \right)_{E_n=E_p} \quad (8)$$

In practice, the quantity actually being measured is  $dN_p/dE_B$  (where  $E_B$  is the energy of the beta particles resulting from Compton recoils) because the light output is not linear with respect to  $E_p$  (see ref. 41). To remedy this, rewrite  $dN_p/dE_p$  as  $(dN_p/dE_B)(dE_B/dE_p)$ ; thus

$$\phi(E_n) = - \frac{E_n}{A\epsilon(E_n)} \left[ \frac{d}{dE_p} \left( \frac{dN_p}{dE_B} \frac{dE_B}{dE_p} \right) \right]_{E_p=E_n} \quad (9)$$

The values of  $dE_B/dE_p$  were computed from reference 41, which gives the relation between  $E_B$  and  $E_p$  for NE 213. Since the  $E_B - E_p$  relation for NE 218 is essentially the same as for NE 213, these computed values of  $dE_B/dE_p$  were used to analyze the NE 218 data.

The TUNS computer program finds the differential neutron spectrum by solving equation (9) above and includes a correction for multiple scattering and wall effects.

The data from a recoil-proton pulse height spectrum were reduced by grouping the counts into bins of five channels each, giving 22 data points. These data were further smoothed to ensure a monotonic decrease in the pulse height spectra (to prevent negative fluxes from appearing in the

output differential neutron spectrum). The program requires input of counts per channel, energies associated with each channel, values of  $dE_B/dE_p$  channel width, live time, scintillator dimensions, and hydrogen concentration. The output is given in terms neutron energy, flux, and statistical error.

### Neutron Spectra

*Bonner sphere data analysis*— Sufficient data were obtained with the Bonner spheres to enable a preliminary evaluation of the cosmic-ray-produced neutron spectrum at an altitude of 12.5 km (41,000 ft) in the energy region from thermal to a few MeV.

Table 9 summarizes measurements made using Bonner spheres of diameters up to 45.7 cm (18-in.) during flight 3. There is presently some unresolved difficulty in incorporating the 45.7 cm (18-in.) moderator data. Incorporation of the counting rate of this sphere and the response function calculated by Sanna (ref. 26) give a neutron spectrum elevated at energies above 20 MeV (fig. 22). If the spectrum is calculated with the 45.7 cm (18-in.) moderator data omitted, as in figure 23, there is no such elevation. Neither the Monte Carlo spectrum, calculated by Merker (ref. 46) and also shown in figure 23, nor the Hess spectrum plotted in figure 24 show such a large increase at higher energies. There are two possible explanations for these differences. Either the 45.7 cm (18-in.) diameter moderator calculated response function is incorrect or there is indeed a shoulder in the neutron spectrum around 10 MeV. Further work is needed before any firm conclusions may be drawn as to the precise nature of the neutron spectrum above a few MeV.

TABLE 9.— BONNER SPHERE MEASUREMENTS — FLIGHT 3

Detector	Measured responses <sup>a</sup>	Calculated responses <sup>b</sup>
1.3 cm (0.5-in.)-LiI		
Bare	51	51
Cd covered	34	34
5.1 cm (2-in.)-PE <sup>c</sup>	119	117
7.6 cm (3-in.)-PE	198	202
12.7 cm (5-in.)-PE	271	271
20.3 cm (8-in.)-PE	186	185
25.4 cm (10-in.)-PE	145	139
30.5 cm (12-in.)-PE	98	102
45.7 cm (18-in.)-PE	56	56

<sup>a</sup>Measured responses; counting rates normalized to 1000 cpm of BF<sub>3</sub> neutron monitor.

<sup>b</sup>Calculated responses; counting rates to be expected for each detector from the assumed spectrum and known response functions.

<sup>c</sup>Polyethylene.

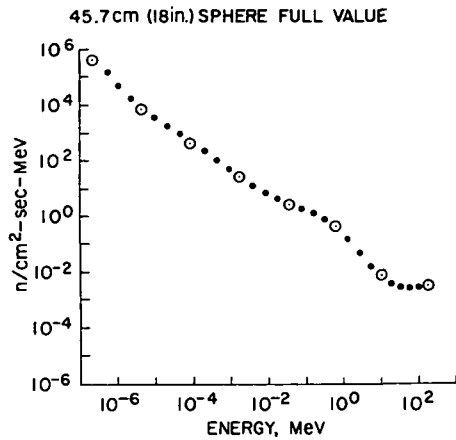


Figure 22.— Differential neutron spectrum from Bonner spheres.

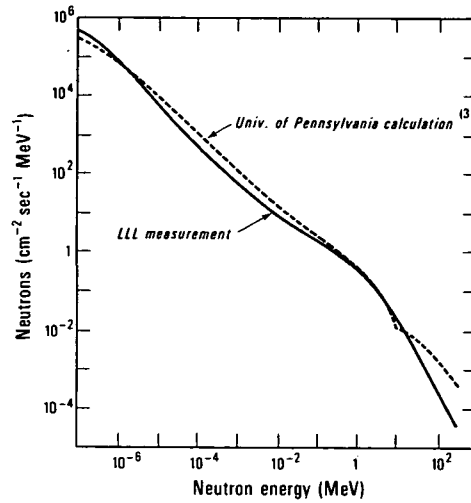


Figure 23.— Comparison of cosmic-ray spectra. Comparison of Bonner sphere spectrum with Merker spectrum (ref. 46).

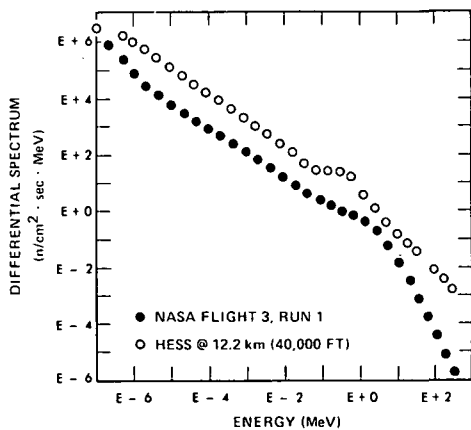


Figure 24.— Comparison of Bonner spheres spectrum with Hess spectrum.

An experimental study of the 45.7-cm (18-in.) diameter sphere response as a function of neutron energy is planned to answer the first alternative. An “evaporation bump” or shoulder in the 1–10-MeV region would not be well resolved with Bonner spheres alone and, consequently, additional data obtained from activation detectors using  $^{27}\text{Al}(n,\alpha)^{24}\text{Na}$ ,  $^{12}\text{C}(n,2n)^{11}\text{C}$  and  $^{209}\text{Bi}(n, \text{fission})$  reactions are important. Preliminary data using the aluminum threshold reaction do not resolve the choice between these two alternatives. More data from other detectors are necessary.

Table 10 shows the calculated responses of the detectors in the Hess spectrum.

TABLE 10.— CALCULATED RESPONSE OF NEUTRON DETECTORS IN THE HESS SPECTRUM

Detector	Relative response
Bare Li	202
Cadmium covered Li	161
5.1 cm (2-in.) moderator	975
7.6 cm (3-in.) moderator	1870
12.7 cm (5-in.) moderator	2540
20.3 cm (8-in.) moderator	1590
25.4 cm (10-in.) moderator	1090
30.5 cm (12-in.) moderator	677
45.7 cm (18-in.) moderator	190
$^{27}\text{Al} (n, \alpha)^{24}\text{Na}$	17.9
$^{12}\text{C}(n, 2n)^{11}\text{C}$	5.3
Bi (n, fission)	0.7

Figure 24 compares the Hess spectrum at 12.2 km (40,000 ft) with the spectrum derived from the present measurements, excluding that from the 45.7-cm (18-in.) sphere. While the results are preliminary, based on one 2-hr flight at constant geomagnetic latitude, they indicate that the fluxes shown in the Hess spectrum may be too high by a factor of 10. Figure 23 compares the Merker spectrum (ref. 46) and the present spectrum, again excluding the measurement with the 45.7-cm (18-in.) sphere. The Merker calculations were made for an altitude of 17 km (55,800 ft) while the present measurements were at 12.5 km (41,000 ft). However, Merker's calculations show that at these two altitudes the fluxes should be less than a factor of 2 apart and this seems to be the case.

#### Liquid Scintillation Detector Data Analysis

The data recorded during the constant geomagnetic leg ( $50.7^\circ$  N) consist of six separate runs. Table 11 indicates the counting rate and corresponding fluxes measured for the constant geomagnetic leg during six time intervals, flown on flight 3 in October 1974. Runs 1 and 2 were made

TABLE 11.— LIQUID SCINTILLATION DETECTOR DATA  
[Constant Geomagnetic Leg:  $50.7^\circ$  N]

Altitude-179 mb

Run time, min	Run 1	Run 2	Run 3	Run 4	Run 5	Run 6
	10	10	20	40	60	40
Counts/min	$20 \pm 2$	$28 \pm 2$	$32 \pm 2$	$40 \pm 2$	$29 \pm 2$	$31 \pm 2$
Flux 3-13 MeV in $\text{n}/\text{cm}^2 \text{ sec}$	0.21	0.30	0.34	0.43	0.31	0.33
$P_c = 2.4 \text{ GV}$	—	—	—	—	—	—

while the aircraft was ascending. Runs 3 to 6 are measurements taken at 12.5 km (41,000 ft) pressure altitude (see table 11).

Figure 25 is the output of the TUNS program showing the differential neutron flux as a function of neutron energy over an interval of 3–10 MeV. Included on the graph (dashed line) is a spectrum with a dependence of the form  $E^{-1.23}$ , taken from the work of Merker et al. (ref. 47) and found by them to apply at high altitudes and to be independent of latitude.

The poor statistics associated with low count rate at altitude resulted in a proton-recoil pulse height spectrum which, when “unfolded” produced an oscillatory neutron spectrum. The oscillations were reduced by integrating the flux under the curve over 1-MeV intervals and plotting the integral value at the average energy for each interval (fig. 25).

Figure 26 shows the count rate during the approximately constant geomagnetic leg as well as the geomagnetic latitude, corrected by higher order spherical harmonic terms (ref. 48). Note that the increase in  $\text{BF}_3$  counting rate observed during the “constant” geomagnetic leg (fig. 16) may be accounted for by these corrections. The solid lines correspond to the time during which the counts were being taken, starting with run 3 and ending with run 6. The average count rate, 33 cpm, remains steady throughout the leg of the flight except for run 4, which was anomalously high and does not correspond with changes in flux recorded by the moderated  $\text{BF}_3$  counter (see fig. 17).

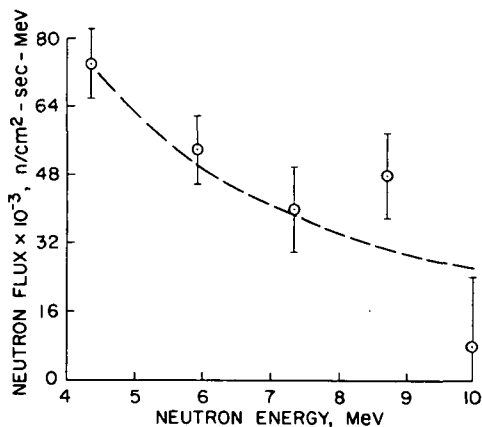


Figure 25.— Differential neutron energy spectrum from LSD: points with error bars are data taken along constant geomagnetic leg and unfolded using TUNS; dashed line spectrum of form  $E^{-1.23}$  from reference 46.

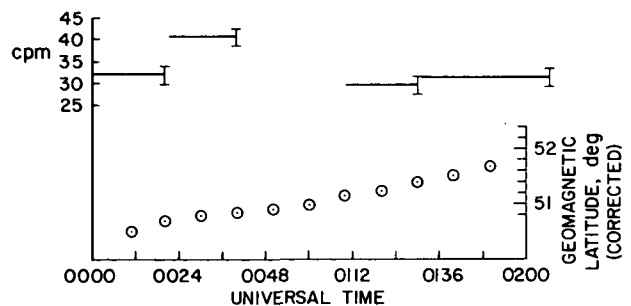


Figure 26.— Data from LSD showing trend in counting rate and deviation of flight path from ideal constant geomagnetic leg.

## SUMMARY AND CONCLUSIONS

Three flights at a pressure altitude of 12.5 km (41,000 ft) were used to test the reliability of several instruments flown to obtain data in the Cosmic Ray Collaborative Study. In addition, preliminary data were obtained which permit some tentative conclusions to be drawn.

The Reuter-Stokes ionization chamber gave exposure rates in the range 300–410  $\mu R/hr$  at altitude during the three flights.

Absorbed dose rates at altitude were measured with the Brookhaven dose equivalent meter to be in the range 275–350  $\mu rad/hr$  with an average of quality factor of 1.8. The neutron component was calculated to be 12 percent of the absorbed dose and 48 percent of the dose equivalent.

Measurements with the moderated  $BF_3$  counter gave values of neutron flux density from 1.09  $n/cm^2$ -sec to 2.28  $n/cm^2$ -sec in the energy range from about 20 keV to 20 MeV at altitude during the flights, while measurements with the aluminum threshold detectors gave a range of 0.32 to 0.50  $n/cm^2$ -sec for the flux density of neutrons greater than 6 MeV.

Exposure, absorbed dose, and dose equivalent rates vary with altitude and geomagnetic latitude. The neutron flux density measured by the moderated  $BF_3$  counter appears to show significantly larger variations than the RS-111 ionization chamber readings at middle geomagnetic latitudes (fig. 16). The ionization chamber readings decrease exponentially with decreasing pressure altitude with an attenuation coefficient of 140  $gm/cm^2$  and vary with geomagnetic latitude,  $\lambda$ , according to the functional form: Exposure rate =  $k (1 - \cos^4 \lambda)$  (fig. 15).

Neutron detectors were carried on three flights to test their performance and reliability in flight. The progress to date may be summarized as

1. Flight monitors: A flight monitor using polyethylene-moderated manganese was developed. The monitor has adequate sensitivity for flights of duration  $\sim 4$  hr. The integrated neutron fluence may be determined with a precision of  $\sim 1$  percent. For active counters, such as Bonner spheres, the moderated  $BF_3$  counter provides a convenient monitor. At an altitude of 12.5 km (41,000 ft) its counting rate is 650 to 1000 counts  $min^{-1}$  and good statistical precision is obtained in measurements of about 10 min duration.

2. Aluminum activation detectors: The  $^{24}Na$  activity induced in the aluminum samples by the  $^{27}Al (n,\alpha) ^{24}Na$  reaction during a flight of  $\sim 5$  hr duration may be measured to an accuracy of  $\sim 5$  percent with the present counting system. The addition of a  $\mu$ -meson anticoincidence shield to the low background counting room  $\gamma$ -spectrometer will facilitate measurements to an accuracy of better than 3 percent. As discussed under Bonner Sphere Data Analysis, the addition of data from the aluminum threshold detector is important in determining the precise shape of neutron spectrum in the 10-MeV region.

3. Bonner spheres: Fission foil detectors have adequate sensitivity for sphere diameters between 7.6 cm (3 in.) and 30.5 cm (12 in.). However, the foil data was not used to unfold spectra because accurate response functions for these detectors are not yet available. When the LiI scintillator is used in flight, the detector pulse height spectrum must be examined to discriminate against the photon and charged-particle background. Measurements of adequate precision can be achieved using all these spheres in a 2-hr flight. Sufficient data have been obtained with the Bonner spheres to enable a preliminary evaluation of the cosmic-ray-produced neutron spectrum at an elevation of 12.5 km (41,000 ft) in the energy region from thermal to a few Mev.

Figure 23 shows the neutron spectrum unfolded using the LOUHI code with all the Bonner sphere data included, except that from the 18-in.-diam moderator. For comparison, a spectrum

calculated using a Monte Carlo technique by Merker (ref. 47) is shown in the same figure. A similar comparison is made with the Hess spectrum in figure 24. Further work is needed before any firm conclusions may be drawn. Inclusion of the data for the 45.7 cm (18-in.) diameter moderator results in large differences at energies above 20 MeV with the spectrum given in figure 22. There are two possible explanations for these differences. Either the calculated response function for the 45.7 cm (18-in.) diameter moderator is incorrect or there is indeed a shoulder in the neutron spectrum around 10 MeV.

An experimental study of the 45.7 cm (18-in.) diameter sphere response as a function of neutron energy is planned to answer the first alternative. An "evaporation bump" or shoulder in the 1–10-MeV region would not be well resolved with Bonner spheres alone and, consequently, additional data obtained from detectors using the  $^{27}\text{Al}(n,\alpha)^{24}\text{Na}$ ,  $^{12}\text{C}(n,2n)^{11}\text{C}$ , and  $^{209}\text{Bi}(n,\text{fission})$  reactions are important. Preliminary data using the aluminum threshold reaction do not resolve the choice between these two alternatives. More data from other detectors are necessary before a firm conclusion may be drawn.

The liquid scintillation detector provided information on both flux and spectral shape of the fast neutron component in the energy range 3 to 13 MeV. The data taken along the constant geomagnetic leg produced a spectrum consistent with that of Merker et al. (ref. 47) with a spectral index of 1.23.

The flux of neutrons for the 3–13 MeV region, when corrected for latitude, pressure altitude, and energy range, gave values of flux intensity that agree closely with the results of Armstrong et al. (ref. 20). Uncertainty in the flux was about 20 percent. No corrections were made to account for the effect of the aircraft on the neutron count rate, which was assumed to be negligible.

Ames Research Center

National Aeronautics and Space Administration

Moffett Field, California 94035, August 1, 1975

## REFERENCES

1. Anon.: Ionizing Radiation: Levels and Effects, Vol. 1 – Levels, United Nations, Scientific Committee on the Effects of Atomic Radiation, New York, Supplement 25, 1972.
2. Hess, W. N.; Canfield, E. H.; and Lingenfelter, R. E.: Cosmic-Ray Neutron Demography. *Journal of Geophysical Res.*, vol. 6, no. 3, March 1961, pp. 665–677.
3. Upton, A. C.; Chase, H. B.; Hekhuis, G. L.; Mole, R. H.; Newcombe, H. B.; Robertson, J. S.; Schaeffer, H. J.; Snyder, W. S.; Sondhaus, C.; Wallace, R.: Radiobiological Aspects of the Supersonic Transport, *Health Physics*, vol. 12, Feb. 1966, pp. 209–226.
4. Hess, W. N.; Patterson, H. W.; Wallace, R. W.; and Chupp, E. L.: Cosmic-Ray Neutron Energy Spectrum, *Phys. Rev.*, vol. 116, no. 2, Oct. 15, 1959, pp. 445–457.

5. Preszler, Alan M.; Sinnett, George M.; and White, R. Stephen: Angular Distribution and Altitude Dependence of Atmospheric Neutrons from 10 to 100 MeV, *J. Geophys. Res.*, vol. 79, no. 1, Jan. 1, 1974, pp. 17-22.
6. Kanbach, G.; Reppin, C.; and Schoenfelder, V.: Support for CRAND Theory from Measurements of Earth Albedo Neutrons Between 70 and 250 MeV, *J. Geophys. Res.*, vol. 79, Dec. 1, 1974, pp. 5159-5165.
7. Jenkins, R. W.; Ifedili, S. O.; Lockwood, J. A.; and Razdan, H.: The Energy Dependence of the Cosmic-Ray Neutron Leakage Flux in the Range of 0.01-10 MeV, *J. Geophys. Res.*, vol. 76, no. 31, Nov. 1, 1971, pp. 7470-7478.
8. Hajnal, Ferenc; McLaughlin, James E.; Weinstein, Martin S.; O'Brien, Keran: 1970 Sea-Level Cosmic-Ray Neutron Measurements, USAEC Rept. HASL-241, Feb. 1971.
9. Anon: Report of the United Nations Scientific Committee on the Effects of Atomic Radiation. General Assembly, Official Records: 21st Session, Supplement 14 (A/6314). United Nations Scientific Committee on the Effects of Atomic Radiation, New York, 1966.
10. Boella, G.; Antoni, G. Degli; Dilworth, C.; Giannelli, G.; Rocca, E.; Scarsi, L.; and Shapiro, D.: Measurement of the Cosmic-Ray Neutron Flux in the Atmosphere, *Il Nuovo Cimento*, vol. 29, no. 1, July 1, 1963, pp. 103-117.
11. Boella, G.; Antoni, G. Degli; Dilworth, C.; Panetti, M.; and Scarsi, L.: Measurement of the Cosmic Ray Neutron Flux at 4.6 Billion Volts Geomagnetic Cutoff Rigidity, *J. Geophys. Res.*, vol. 70, no. 5, March 1, 1965, pp. 1019-1030.
12. Watt, D. E.; Clare, D. M.; Gordon, A. R. B: Tissue Dose-Equivalent Rates. I. From Cosmic Ray Neutrons. II. In the Low Level Environment of Chapelcross Nuclear Power Station. UKAEA Rept. PG-Report-734, 1965.
13. Kent, R. A. R.: Cosmic Ray Neutron Measurements, USAEC Rept., HW-SA-2870, May 25, 1963.
14. Yamashita, Mikio; Stephens, Lloyd D.; and Patterson, H. Wade: Cosmic-Ray-Produced Neutrons at Ground Level: Neutron Production Rate and Flux Distribution, *J. Geophys. Res.*, vol. 71, no. 16, Aug. 15, 1966, pp. 3817-3834.
15. Simpson, J. A.: Neutrons Produced in the Atmosphere by the Cosmic Radiations, *Phys. Rev.*, vol. 83, no. 6, Sept. 15, 1951, pp. 1175-1188.
16. O'Brien, Keran; and Burke, Gail de P.: Calculated Cosmic Ray Neutron Monitor Response to Solar Modulation of Galactic Cosmic Rays, *J. Geophys. Res.*, vol. 78, no. 16, June 1, 1973, pp. 3013-3019.
17. Lowder, W. M.; Raft, P. D.; and Beck, H. L.: Experimental Determinations of Cosmic-Ray Charged Particle Intensity Profile in the Atmosphere. Proceedings of National Symposium on Natural and Man-Made Radiation in Space, (E. A. Worman, ed.), NASA TM X-2440, Jan. 1972.
18. Patterson, H. W.; Hess, W. N.; Moyer, B. J.; and Wallace, R. W.: The Flux and Spectrum of Cosmic-Ray Produced Neutrons as a Function of Altitude, *Health Physics*, vol. 2, July 1959, pp. 69-72.
19. O'Brien, K.: Cosmic-Ray Propagation in the Atmosphere, *Il Nuovo Cimento*, vol. 3A, no. 3, June 1, 1971, pp. 521-547.

20. Armstrong, T. W.; Chandler, K. C.; and Barish, J.: Calculations of Neutron Flux Spectra Induced in the Earth's Atmosphere by Galactic Cosmic Rays, *Journal of Geophys. Res.*, vol. 78, no. 16, June 1, 1973, pp. 2715-2726.
21. Merker, M.: Contribution of Galactic Cosmic Rays to the Atmospheric Neutron Maximum Dose Equivalent as a Function of Neutron Energy and Altitude, *Health Physics*, vol. 25, no. 5, Nov. 1973, pp. 524-527.
22. Thomas, R. H.: Neutron Dosimetry at High-Energy Particle Accelerators. Neutron Monitoring for Radiation Protection Purposes. Vol. 1. International Atomic Energy Agency, Vienna, 1973, pp. 327-353.
23. Cameron, R. M.; Bader, M. S.; and Mobley, R. E.: Design and Operation of the NASA 91.5-cm Airborne Telescope, *Applied Optics*, vol. 10, no. 9, Sept. 1971, pp. 2011-2015.
24. Bramblett, Richard L.; Erving, Ronald I.; and Bonner T. W.: A New Type of Neutron Spectrometer, *Nucl. Instruments Methods*, vol. 2, Oct. 1960, pp. 1-12.
25. Cross, W. G.; and Tommasino, L.: Rapid Reading Technique for Nuclear Particle Damage Tracks in Thin Foils, *Proceedings of the International Topical Conference on Nuclear Track Registration in Insulating Solids and Applications*, Clermont-Ferrand, France, May 6-9, 1969. D. Isabelle, editor. Clermont-Ferrand, France, Universite de Clermont-Ferrand, 1969.
26. Sanna, R. S.: Thirty-one Group Response Matrices for the Multisphere Neutron Spectrometer Over the Range Thermal to 400 MeV, USAEC Health and Safety Laboratory Rept. HASL-267, March 1973.
27. Smith, A. R.: Threshold Detector Applications to Neutron Spectroscopy at the Berkeley Accelerators, *Proceedings of USAEC First Symposium on Accelerator Radiation and Experience*, Brookhaven National Lab., Nov. 3-5, 1965, pp. 365-409.
28. Gilbert, William S.; Shaw, Kenneth B.; Fortune, Ronald D., et al.: 1966 CERN-RL-RHEL Shielding Experiment at the CERN Proton Sychrotron. UCRL-17941, Sept. 1968.
29. Baum, J. W.: Nonlinear Amplifier for Use in Mixed Radiation Rem Responding Radiation Meters. *Health Physics*, vol. 13, July 1967, pp. 775-781.
30. Baum, John W.; Woodcock, Ray C.; and Kuehner, Alan V.: Factors Affecting Pulse Size in Sealed Tissue-Equivalent Counters. BNL-14063, Presented at the 2nd International Conference on Accelerator Dosimetry and Experience, Stanford, Calif., Nov. 5-7, 1969.
31. Kuehner, A. V.; Chester, J. D.; and Baum, J. W.: Portable Mixed Radiation Dose Equivalent Meter. *Neutron Monitoring for Radiation Protection Purposes*, vol. 1, International Atomic Energy Agency, Vienna, 1973, pp. 233-246
32. Rossi, Harold H.; and Rosenzweig, Walter: Measurements of Neutron Dose as a Function of Linear Energy Transfer. *Rad. Res.*, vol. 2, July 1955, pp. 417-425.
33. Benjamin, P. W.; Kemshall, C. G.; and Redfearn, J.: A High-Resolution Spherical Proportional Counter. UKAEA Rept. AWRE-NR-1/64, June 1964.
34. DeCampo, J. A.; Beck, H. L.; and Raft, P. D.: High Pressure Argon Ionization Chamber Systems for the Measurement of Environmental Radiation Exposure Rates. USAEC Rept. HASL-260, Dec. 1972.
35. Kuchnir, Franca T.; and Lynch, Frank J.: Time Dependence of Scintillation and the Effect of Pulse-Shape Discrimination, *IEEE Trans. Nucl. Sci.*, vol. NS-15, no. 3, June 1968, pp. 107-113.

36. Mendell, R. B.; and Korff, S. A.: A Fast-Neutron Detector with Discrimination Against Background Radiation, *Rev. Sci. Instr.*, vol. 34, no. 12, Dec. 1963, pp. 1356–1360.
37. Daehnick, W.; and Sherr, R.: Pulse Shape Discrimination in Stilbene Scintillators, *Rev. Sci. Instr.*, vol. 32, no. 6, June 1961, pp. 666–670.
38. Burrus, W. R.; and Verbinski, V. V.: Fast-Neutron Spectroscopy with Thick Organic Scintillators, *Nuclear Instruments and Methods*, vol. 67, no. 2, Jan. 15, 1969, pp. 181–196.
39. Shook, D. F.; and Pierce, C. R.: Comparison of Neutron Spectra Measured with Three Sizes of Organic Liquid Scintillators using Differential Analysis, NASA TM X-2646, 1972.
40. Pohl, B. A.; Anderson, J. D.; McClure, J. W.; and Wong, C.: Method for Determining Scintillator Response Function for Fast Neutrons, Lawrence Radiation Lab. Rept. UCRL-50653, April 29, 1969.
41. Verbinski, V. V.; Burrus, W. R.; Love, T. A.; Zobel, W.; and Hill, N. W.: Calibration of an Organic Scintillator for Neutron Spectrometry, *Nuclear Instruments and Methods*, vol. 65, no. 1, Oct. 15, 1968, pp. 8–25.
42. Flynn, K. F.; Glendenin, L. E.; Steinberg, E. P.; and Wright, P. M.: Pulse Height-Energy Relations for Electrons and Alpha Particles in a Liquid Scintillator, *Nuclear Instruments and Methods*, vol. 27, no. 1, April 1964, pp. 13–17.
43. Patterson, H. W.; Routti, J. T.; and Thomas, R. H.: What Quality Factor? *Health Phys.*, vol. 20, 1971, p. 517.
44. O'Brien, Keran; and McLaughlin, James E.: The Radiation Dose to Man from Galactic Cosmic Rays. *Health Phys.*, vol. 22, March 1972, pp. 225–232.
45. Routti, Jorma T.: High-Energy Neutron Spectroscopy with Activation Detectors, Incorporating New Methods for the Analysis of Ge(Li) Gamma-Ray Spectra and the Solution of Fredholm Integral Equations. UCRL-18514, 1969.
46. Merker, M.: Contribution of Galactic Cosmic Rays to the Atmospheric Neutron Maximum Dose Equivalent as a Function of Neutron Energy and Altitude, *Health Physics*, vol. 25, Nov. 1973, pp. 524-527.
47. Merker, M.; Light, E. S.; Verschell, H. J.; Mendell, R. B.; and Korff, S. A.: Time Dependent Worldwide Distribution of Atmospheric Neutrons and of Their Products. Part I. Fast Neutron Observations. *J. Geophys. Res.*, vol. 78, no. 16, June 1, 1973, pp. 2727–2740.
48. Hakura, Yukio: Tables and Maps of Geomagnetic Coordinates Corrected by the Higher Order Spherical Harmonic Terms: Report of Ionosphere and Space Research in Japan, vol. 19, 1963, pp. 133–144.



POSTMASTER : If Undeliverable (Section 158  
Postal Manual) Do Not Return

*"The aeronautical and space activities of the United States shall be conducted so as to contribute . . . to the expansion of human knowledge of phenomena in the atmosphere and space. The Administration shall provide for the widest practicable and appropriate dissemination of information concerning its activities and the results thereof."*

—NATIONAL AERONAUTICS AND SPACE ACT OF 1958

## NASA SCIENTIFIC AND TECHNICAL PUBLICATIONS

**TECHNICAL REPORTS:** Scientific and technical information considered important, complete, and a lasting contribution to existing knowledge.

**TECHNICAL NOTES:** Information less broad in scope but nevertheless of importance as a contribution to existing knowledge.

**TECHNICAL MEMORANDUMS:** Information receiving limited distribution because of preliminary data, security classification, or other reasons. Also includes conference proceedings with either limited or unlimited distribution.

**CONTRACTOR REPORTS:** Scientific and technical information generated under a NASA contract or grant and considered an important contribution to existing knowledge.

**TECHNICAL TRANSLATIONS:** Information published in a foreign language considered to merit NASA distribution in English.

**SPECIAL PUBLICATIONS:** Information derived from or of value to NASA activities. Publications include final reports of major projects, monographs, data compilations, handbooks, sourcebooks, and special bibliographies.

**TECHNOLOGY UTILIZATION PUBLICATIONS:** Information on technology used by NASA that may be of particular interest in commercial and other non-aerospace applications. Publications include Tech Briefs, Technology Utilization Reports and Technology Surveys.

*Details on the availability of these publications may be obtained from:*

**SCIENTIFIC AND TECHNICAL INFORMATION OFFICE**

**NATIONAL AERONAUTICS AND SPACE ADMINISTRATION**  
Washington, D.C. 20546